Lawrence Berkeley National Laboratory

Lawrence Berkeley National Laboratory

Title

Pump probe spectroscopy of quasiparticle dynamics in cuprate superconductors

Permalink

https://escholarship.org/uc/item/1kr389qh

Author

Segre, Gino P.

Publication Date

2001-05-01

eScholarship.org Powered by the California Digital Library
University of California

Pump Probe Spectroscopy of Quasiparticle Dynamics in Cuprate Superconductors

by

Gino Paolo Segrè

B.A. (University of California, Berkeley) 1992
M.A. (University of California at Berkeley) 1995

A dissertation submitted in partial satisfaction of the
requirements for the degree of
Doctor of Philosophy

in

Physics

in the

GRADUATE DIVISION
of the
UNIVERSITY of CALIFORNIA at BERKELEY

Committee in charge:

Professor Joseph Orenstein, Chair
Professor Daniel Chemla
Professor Kenneth Gustafson

Spring 2001

Pump Probe Spectroscopy of Quasiparticle Dynamics in Cuprate Superconductors

Copyright 2001

by

Gino Paolo Segrè

Abstract

Pump Probe Spectroscopy of Quasiparticle Dynamics in Cuprate Superconductors

by

Gino Paolo Segrè

Doctor of Philosophy in Physics

University of California at Berkeley

Professor Joseph Orenstein, Chair

Pump probe spectroscopy is used to examine the picosecond response of a $Bi_2Sr_2CaCu_2O_8$ thin film, and two $YBa_2Cu_3O_7$ crystals in the near infrared. The role of pump fluence and temperature have been closely examined in an effort to clarify the mechanism by which the quasiparticles rejoin the condensate. $Bi_2Sr_2CaCu_2O_8$ results suggest that the recombination behavior is consistent with the *d*-wave density of states in that quasiparticles appear to relax to the nodes immediately before they rejoin the condensate.

The first substantial investigation of polarized pump-probe response in detwinned YBCO crystals is also reported. Dramatic doping dependent anisotropies along the *a* and *b* axes are observed in time and temperature resolved studies. Among many results, we highlight the discovery of an anomalous temperature and time dependence of *a*- axis response in optimally doped YBCO.

We also report on the first observation of the photoinduced response in a magnetic

field. We find the amplitude of the response, and in some cases, the dynamics considerably changed with the application of a 6T field.

Finally, we speculate on two of the many theoretical directions stimulated by our results. We find that the two-fluid model suggests a mechanism to explain how changes at very low energies are visible to a high-energy probe. Also discussed are basic recombination processes which may play a role in the observed decay.

Professor Joseph Orenstein
Dissertation Committee Chair

Contents

List of Figures **vi**

1 Introduction **1**

2 Pump Probe Spectroscopy **3**
2.1 Optics 4
2.2 Cryostats 5
2.3 Instrumental Complications 7

3 Elements of Superconductivity **10**

4 Historical Review of Pump Probe Techniques **15**

5 $Bi_2Sr_2CaCu_2O_{8+\delta}$ and the Nodal Quasiparticle Picture **26**
5.1 Temperature and Intensity Dependence 27
5.2 Analysis of Decay Rate 29
5.3 Nodal Quasiparticle Density of States 31

6 $YBa_2Cu_3O_x$ **34**
6.1 Temperature and Intensity Dependence of Two Dopings 35

7 Magnetic Field Effects **39**
7.1 Neutron Scattering and the Picosecond Response 39
7.2 Neutron Scattering in a Field 41
7.3 Picosecond Response in a Field 42

8 Theoretical Models **46**
8.1 Two-Fluid Model and Optical Frequency Response 46
8.2 Recombination Mechanisms 49

9 Summary and Future Directions **52**

Bibliography **56**

A Aligning Tips **63**
A.1 Delay Lines 63
A.2 Finding the Overlap 64

B Supplementary Data **66**

List of Figures

2.1 Optical Schematic of Apparatus 5

3.1 *d*-wave and *s*-wave parameter compared. 11
3.2 YBCO unit cell 12
3.3 Generic phase diagram. 13
3.4 YBCO: Reflectivity 0-5eV. 14

4.1 YBCO: Differential Photothermal Reflectivity 20
4.2 Optimal YBCO: Temperature dependence along *aa* direction. 20
4.3 Comparison of Thermal Difference Spectroscopy with Pump Probe Technique 21
4.4 Pump Probe Spectroscopy in the Infrared 22
4.5 Pump Probe Spectroscopy Compared with Stationary Reflectivity 23

5.1 BSCCO: Temperature dependence of ΔR/R *vs* time 27
5.2 BSCCO: Decay Rate for Different Pump Intensities 28
5.3 BSCCO: Linearity of Response 29
5.4 BSCCO: The extracted decay rate plotted *vs* ΔR/R. 30
5.5 BSCCO: Scaling behavior suggests Nodal QPDOS 32
5.6 *d*-wave Nodal Density of States 32

6.1 Underdoped YBCO: Intensity dependence 36
6.2 Optimal YBCO: Intensity dependence 36
6.3 Optimal YBCO: Polarization and temperature Response 37
6.4 Underdoped YBCO: Polarization and temperature Response 37
6.5 Optimal YBCO: Temperature dependence along *aa* and *bb* directions. . . . 38
6.6 Underdoped YBCO: Temperature dependence along *aa* and *bb* directions. . 38

7.1 Picosecond data compared with neutron scattering. 40
7.2 Underdoped YBCO: Temperature dependence of neutron resonance. 43
7.3 Underdoped YBCO: Temperature dependence of B-field response 43
7.4 Underdoped YBCO: Temperature dependence of B-field response 43
7.5 Optimal YBCO: Field strongly influences dynamics along *a*- axis. 45

8.1 YBCO reflectivity data to 2000cm^{-1} 48
8.2 Two Fluid Model: A mechanism for the response at 1.5eV 49
8.3 YBCO: Decay rate *vs* pump fluence 51

B.1 Optimal BSCCO plotted on a semilog axis. 67
B.2 YBCO: Peak response *vs* pump fluence 68
B.3 YBCO: Influence of pump fluence on temperature dependence. 69
B.4 YBCO: Decay rate *vs* Temperature 70

Acknowledgements

An advanced degree is often an arduous journey. Fortunately it is not a lonely one, I have received support in many forms from a number of people who ultimately made the experience what it was.

Rene Delano is an outstanding machinist who interpreted my primitive engineering sketches. Jeff Beeman is a master of all things microscopic and cryogenic who generously provided advice and materials. Steve Dodge is a fountain of knowledge on many things well beyond science, and always has time for my physics. Robert Kaindl is a specialist in my microcosmos and has enriched my understanding of many of its finer points. Nuh Gedik is an enthusiastic and capable successor who amplified my efforts and will carry this field forward smartly. Jim Eckstein's group and Doug Bonn's group are world-class specialists in sample growing who believe in the value of our research. Joe Orenstein, my thesis advisor, provided expertise in superconductivity, and golf, and gave direction with the lightest touch. Donna Sakima and Anne Takizawa made it possible to believe there was no such thing as administration.

Rich Mallozzi, John Corson, Andreas Schumacher, Neil Fromer, Jen Glass, and Peter Kner are all companions in the PhD odyssey who provided expert counsel on things outrageous, comical, silly, cultural, historical, and political. They are all lifetime members of the Slacker Vortex, a "place" where one can go to seek shelter from physics.

Thanks to all of you.

Chapter 1

Introduction

Pump probe spectroscopy has been established as a useful tool to probe dynamical behavior in a wide variety of materials[59], including the high-T_c cuprates. In superconductors the transient change in reflectivity created by a strong pump pulse, and measured by a weak probe, is due to the conversion of superfluid condensate into quasiparticles. Once the energy of the excitation dissipates, the electrons rejoin the condensate. We seek to clarify the mechanisms of this relaxation process through control of a number of experimental variables.

The thesis is organized as follows: We begin in chapters 2 and 3 with an overview of experimental techniques we use and outline the salient features of high-T_c cuprates.

Chapter 4 describes the important advances in this field. In this section we construct a simple picture of how to think about photoinduced response. The evidence available demonstrates that the principal component of the photoinduced reflectivity change is a consequence of the destruction of condensate via an electronic process, not a thermal one.

The role pump fluence has on the dynamical response has received little attention in the literature. Combined with temperature dependence, we have found intensity dependence to be a fruitful investigative direction. In chapter 5, for example we find evidence that quasiparticles relax to the nodes before they rejoin the condensate.

Chapter 6 and 7 comprise the experimental centerpiece of this work, showing the rich variety of phenomena possible in pump probe measurements. In YBCO, different dopings produce large changes in the recombination kinetics. Where optimally doped YBCO appears to be insensitive to pump fluence, underdoped samples show pronounced pump intensity dependence.

In the final chapter, we address perhaps the most fundamental question of all: why do we observe low energy excitations with much higher energy probes? We also speculate on models of recombination which may be used to describe our data.

Editorial Comment: This field is a rather ambitious one to pursue, it applies an exotic technique to probe an exotic material. Pump probe spectroscopy is not yet a mature characterization tool. Furthermore cuprates are among the most studied and complex materials. Thus this subfield is exciting for the same reasons it is daunting, relatively little is well understood. It is the author's sincere hope that this thesis will serve as a useful reference which will stimulate future investigation.

Chapter 2

Pump Probe Spectroscopy

Degenerate pump probe spectroscopy uses the ultrashort pulse output of an ultrafast laser as both pump and probe beams. Traditionally, the pump to probe intensity ratio is much greater than one. By varying the time delay between the pump and probe beam, a picture of the time evolution of the quasiparticle excitation is constructed. Fractional changes in reflectivity as small as 10^{-6} can be measured. Typical signals we observe are at the 10^{-4}-10^{-5} level.

One helpful way to understand the apparatus is to consider the time scales involved in making the measurement. The pulse duration of the laser, 100fsec, should be considerably shorter than the response of the superconductor, 1 psec. Because the roll-off frequency of the photodiode(10MHz) is much lower than the repetition rate of the laser(86MHz), the photodiode integrates the response of the superconductor over many pulses. Employing a photoelastic modulator in conjunction with a lockin amplifier facilitates noise suppression. The intensity modulation occurs at twice the fundamental frequency, 2f=100kHz. The

sweep rate of the optical delay (Clark-MXR ODL-150) line is 40 Hz. Limitations of the oscilloscope only permit acquisition of twenty sweeps per second from every other trigger pulse. Also, the scope acquires only when the delay line is moving in one direction, and is effectively idle when moving in the opposite sense. The lockin time constant is set to 100μsec.

2.1 Optics

We now describe the setup depicted in figure 2.1. The output of a diode pumped (SpectraPhysics Millenia) Ti:Sapphire (KM Labs) laser is split into two beams of unequal intensity. The central wavelength is nominally 800nm. The more intense pump beam is sent to a rapid scan optical delay line. Following the delay line, the beam is sent to a photoelastic modulator (Hinds Instruments PEM-90) whose axis is at 45 degrees to the incident polarization. The modulation amplitude is set to one-half wave. The analyzer (polarizer oriented parallel to the original polarization state of the beam) then modulates the intensity of the beam. A neutral density filter then controls the pump intensity and a half-wave plate controls its polarization. Finally, a steering mirror with fine pitch adjustments, is employed to optimize the overlap. This adjustment can be made in realtime by observing the amplitude of the response on the oscilloscope.

The probe beam is sent to a Klinger stepper, which is only used to obtain a coarse zero time delay between the two beams. It is then directed through the requisite ND filter. A half-wave plate may be introduced to cross polarize the pump and probe beams. Both beams are focussed to a sub-100μ size spot using a doublet achromat lens (f=200mm). The

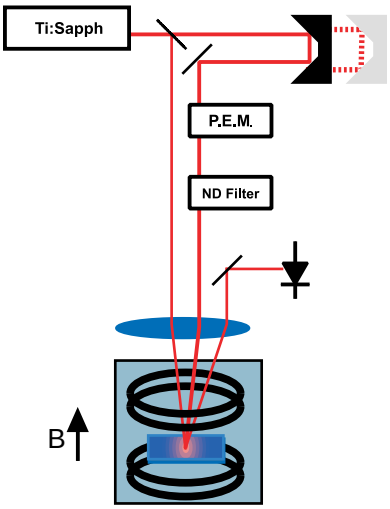

Figure 2.1: Optical Schematic of the apparatus. A discussion of the signal processing is included in the body.

reflected probe beam is then directed to a photodiode. Techniques used to align the optical system are described in the appendix.

2.2 Cryostats

Our first measurements (BSCCO data) were made using a cold-finger cryostat which is convenient because it requires little preparation. It lacks magnetic field and low temperature (<5K) capability however. Measurements of BSCCO were made at an angle of incidence of 45 degrees, for convenience. In this way the light reflected light from the sample does not retrace the path of the incident beam. This angle of incidence also simplifies discrimination of the pump beam from the probe beam. The advantage of such a system is the quick cooldown.

A Janis 12CNDT magnet cryostat is employed to collect all the YBCO data. With this system, what is invested in preparation is returned in capability. Once the tedious

cooldown procedure is complete, 2 Kelvin and 7 Tesla operation are readily obtained.

The entire cryostat is mounted on a translation stage to facilitate fine positioning of the sample in the plane of the optical table. We can also set the pitch or height of the cryostat by adjusting the length of any of its supporting legs. This freedom is an indispensable feature of our apparatus, since the surface of the sample may not be reflecting the beam in a useful direction. We can also remedy situations in which certain parts of the sample may have too much pump scatter. This is a condition in which too much of the pump light is incident on the photodiode and the signal of interest (at 100kHz) is swamped by the modulation of the pump beam at the same frequency. The telltale sign of such a situation is lockin overload.

Inside the magnet cryostat, the temperature is recorded by one of two sensors. One sensor is embedded in the sample stick, and separated from the sample by as much as an inch. This distance has potential to cause error in temperature measurements due to thermal gradients. Thermal gradients are the result heat exchange between the flowing gas and it surroundings. The further it travels the more its temperature deviates from the desired site point. The magnitude of thermal gradients will depend on the set point and the rate at which the sample is being cooled or warmed. A temperature sensor CX-1050(LakeShore) was introduced to monitor the sample temperature more closely. The common configuration is to place it on the opposite side of the substrate to which the sample crystal is attached. Samples and sensors are affixed with N type Apiezon cryogenic grease, or GE-7031 Varnish(LakeShore). All crystals and films are *c*-axis oriented, the electric field orientation of the incident light is always in the *ab* plane.

Electronically the system operates as follows: A signal generator drives the optical delay line via a driver module. The position of the delay line is converted to a voltage by the same driver module and sent to the oscilloscope and serves as the x-axis. The driver module of the photoelastic modulator sends a reference signal to the lockin amplifier, while the output of the photodiode serves as the input signal to the lockin(Stanford Research 850). The output of the lockin amplifier is then sent to the oscilloscope(LeCroy 9310M) and serves as the y-axis. These two channels (x and y) are averaged by the oscilloscope and sent to the computer. Data acquisition software was written in LabWindowsCVI.

There are two modes in which we operate the system. The conventional way is to record temporal information by sweeping the time delay and holding the temperature constant. We can record temperature dependent behavior in very fine steps by setting the delay line to scan from small negative time delay to the peak of the response. The temperature is then allowed to sweep up and down. In this way the peak response is recorded as a function of temperature. Two minutes (400 sweeps) is ordinarily sufficient to obtain a satisfactory time trace. Temperature sweeps take about 30 minutes since we are interested in minimizing error due to thermal gradients. The raw data is then imported and analyzed in Matlab 5.3.

2.3 Instrumental Complications

A number of undesired physical phenomena may be encountered at low temperatures. Below 5K, we observed that helium gas refracts the beam in a chaotic fashion. (Wild fluctuations in the probe DC voltage are a telltale sign.) Through careful manipulation of

the sample cell pressure (via a vacuum pump) and helium flow (via a needle valve) we are able to lower the temperature to less than 2.2K. For the lowest operating temperatures, we find working in a low pressure gas environment preferable to working with superfluid helium. If the liquid level drops below the sample during data acquisition, the optical path is interrupted and the run must be aborted. Working in liquid also requires a consideration of the effects of the change in index of refraction. On the other hand, cooling power may be enhanced.

During temperature-swept data acquisition, the sample often moves. The source of this motion is most likely due to thermal expansion of the sample stick. While the thermal expansion properties do not normally play a role at low temperature, there is always some portion of the sample stick which is changing temperatures in the regime where the coefficient of thermal expansion is non-zero.

We often observe around zero time delay a very sharp feature in the time trace, whose intensity fluctuates rapidly from positive to negative. This is most likely due to interference of the pump and probe beams. The rapid fluctuations are thought to arise from slight wobbles in the optical delay line motion. Generally, this feature can be eliminated by moving the stepper a few microns until the fluctuations are no longer observable. Such features have been observed at times far from zero time delay. Again the origin is probably the same, except with a beam which is reflecting off another surface and creating an interference effect. Cross polarization of the beams can help to eliminate this phenomenon.

Undesirable effects resulting from the application of magnetic fields are also possible. Beam alignment may be thrown off when the inductive forces on the sample stick

change sign. This scenario is common when the field ramp direction is changed. To combat this annoyance, notches were cut in the sample holder (made of OFHC copper) to prevent large inductive current loops from forming.

Since a superconductor behaves as a diamagnet, strong gradients in a magnetic field are an experimental hazard. Large forces can act on a crystal and rip it from its mount. Cooling the sample in a preset magnetic field can reduce the chance this will occur. Following such a protocol also minimizes reproducibility problems associated with flux creep.

Chapter 3

Elements of Superconductivity

BCS theory has been very successful in describing conventional superconductors. Among the major achievements is the identification of the attractive electron-phonon interaction that binds the Cooper pairs together. A direct consequence of this idea is the density of states has a uniform gap energy of 2Δ everywhere in k-space.

While paired electrons are central to superconductivity in the high-T_c cuprates, the BCS description falls short of describing the mechanism in high-T_c materials. One immediate complication is the anisotropic nature of the material. Almost all of the superconductivity resides within the *ab* planes with very weak coupling between planes along the *c* direction.

Recent advances have, ironically, complicated the picture further. Unlike its elemental brethren, cuprates have been shown to have an order parameter with *d*-wave symmetry [69, 72]. Such a pairing symmetry places constraints on the nature of the pairing mechanism. The reader is referred to the literature for a review of prominent theories. A

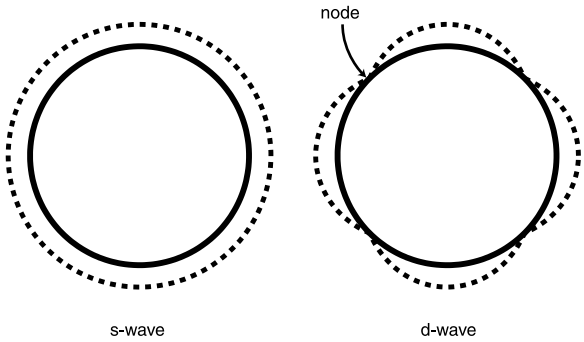

Figure 3.1: A comparison of the magnitude of the gap for s-wave and d-wave order parameters as a function of angle in k-space. The gap magnitude is a linear function of angle for small angular deviations from the node.

concise summary can be found in [37].

Whatever the mechanism, the symmetry of the order parameter has direct consequences for interpretation of our data. This is most plainly seen in figure 3.1. While the s-wave symmetry leads to an isotropic gap, d-wave superconductors are characterized by nodes– directions in k-space for which there is no gap. These nodal regions make possible very low energy excitations.

At finite temperatures, a probability exists that a Cooper pair will dissociate into its constituent unpaired electrons. In BCS formalism the probability of such an event is proportional to $e^{-\Delta/k_bT}$. Exponentially activated thermodynamic, optical and transport properties follow from this property. The presence of nodes in the cuprates means that the number of thermal excitations is proportional to temperature squared. This is further discussed in section 5.3.

All of the high-T_c cuprates are layered perovskite materials. Perhaps the most intensively studied system is YBCO. To fix the discussion, we show the YBCO unit cell in figure 3.2. As previously mentioned, supercurrent flows in the $CuO_2(ab)$ planes. Hole

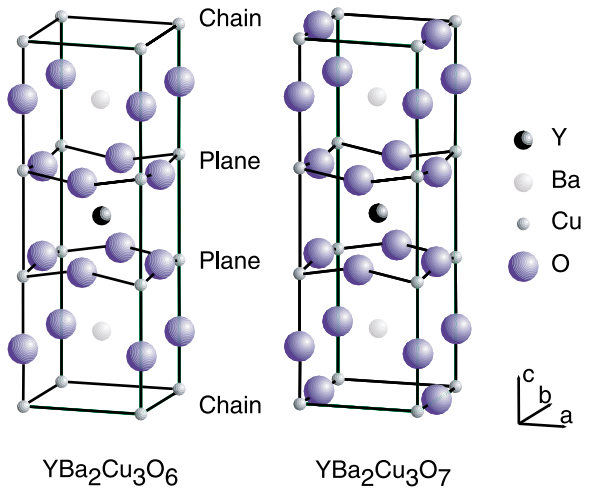

Figure 3.2: The dimensions of the unit cell are roughly 3.8Å × 3.8Å × 11.7Å. On the left is the parent compound, an antiferromagnetic insulator. Note the absence of oxygens in the chains layer. At right is the unit cell near optimal doping, with the chains fully occupied. The presence of chains in YBCO makes makes the *ab* plane orthorhombic. The $O_{6.5}$ phase, discussed later, has every other chain fully occupied.

doping, the most common way to modify electronic properties, is achieved through variation of oxygen content. This changes the occupation of sites in the chains layer (also known as charge reservoir layer) while oxygen sites in the *ab* planes are always fully occupied. Since we present results on BSCCO, we note an important distinction that BSCCO lacks the chains present in YBCO. Oxygen is always present between any two nearest Sr or any two nearest Bi atoms.

The generic cuprate phase diagram, figure 3.3, shows how doping changes the electronic behavior rather dramatically. The samples we study fall into two distinct categories: optimally, and under- doped. For optimal YBCO, T_c is maximum, 93K, at 15% hole concentration. Underdoped contains somewhat less oxygen, and T_c is depressed to 58K for the samples we studied. Above T_c and up to a temperature T^*, underdoped exists in a pseudogap state, a property absent in conventional superconductors. In this regime, a gap forms

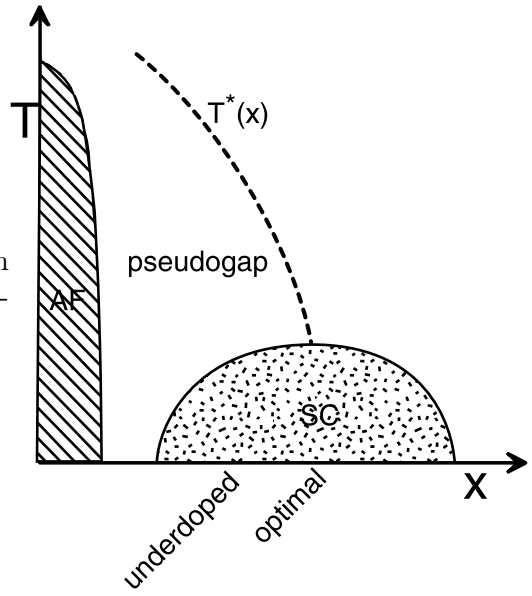

Figure 3.3: Schematic of the variation in electronic properties as a function of oxygen content on the behavior of YBCO.

without the requisite long-range phase coherence but its relation to the superconducting state is unclear. Above T*, the pseudogap disappears.

Anticipating the data we will present, we offer some background on other probes which measure anisotropy (broken four-fold symmetry) in d-wave superconductors. Infrared and microwave experiments on untwinned YBCO crystals have shown that chains play a significant role in the superconductivity. The absolute value of the penetration depth has been measured in infrared experiments [5]. Along the chains, $\lambda_b \sim$1030Å and perpendicular to them $\lambda_a \sim$ 1600Å. The temperature dependence, however, of the normalized penetration depth $\lambda(T)/\lambda(0)$ is nearly identical in both directions [7, 31]. Other reports of anisotropy in the gap magnitude have been reported in photoemission experiments [2].

Optical anisotropy has also been observed. There is a large difference between a- and b- axis reflectivity, suggesting that the chains play a major role in the optical response. We find the reflectivity ratio at 1.5eV is 3:1 ($a : b$) consistent with previous reports [16, 62].

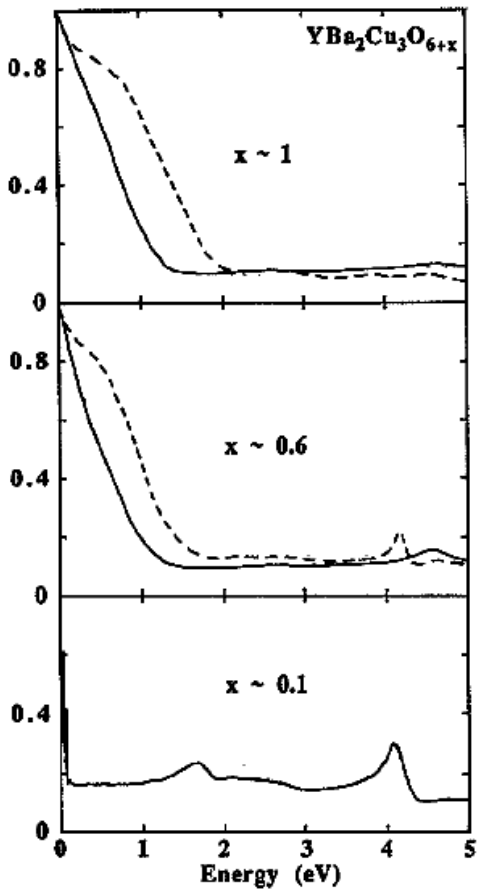

Figure 3.4: Room-temperature reflectivity *vs* frequency for single domain $YBa_2Cu_3O_{6+x}$. x$\sim$0.1; x$\sim$0.6 T_c=66K; x$\sim$1 T_c=90K. Solid (dashed) lines are the reflectivities along a (b)-axis. For x$\sim$0.1, the 1.75eV feature, is the charge transfer gap. From [15].

Unpolarized reflectivity is R$\approx$0.1. Due to the orthorhombic nature of the unit cell, there are two distinct in-plane plasma frequencies to consider: a=1.03$\pm$.11eV and b=1.48$\pm$.15eV [34].

A fair amount is also known about the ordinary spectral response of the cuprates. Upon cooling, the most dramatic changes in optical properties for the cuprates occur in the infrared [57]. For $YBa_2Cu_3O_7$, temperature dependent changes in the visible are about 10 times smaller than in the infrared (see Figure 4.3). It was determined significant deviations around 2.0eV are not unique to $YBa_2Cu_3O_7$, but a common property of a number of cuprates [34].

Chapter 4

Historical Review of Pump Probe Techniques

Presenting general properties of the ultrafast response in cuprates, and identifying the important open questions is the primary goal of this chapter. We provide a selective overview of the literature in rough chronological order. Since the seminal experiments a decade ago, the study of ultrafast properties of the cuprates has grown steadily. The effort has benefitted enormously from the refinement of both laser technology and sample growth techniques. Diode pumped ultrafast lasers are extremely low noise and are turnkey. Sample quality is now outstanding: crystals are well characterized, of high purity, and near perfect ordering.

Primarily dynamics of YBCO have been examined, but BSCCO and $Tl_2Ba_2Ca_2Cu_3O_{10}$ have also been studied. Pump and probe energies have varied from 1 to 3 eV, and very limited continuum studies have been performed[27, 44].

Studies of ultrafast phenomena in superconductors were naturally motivated out of the successes of experiments in metals [59]. Brorson published the first results on YBCO and BSCCO films but only at room temperature [9]. Using differential transmission and reflection techniques their experiments showed an initial fast (250fsec) transient subsequent to optical excitation followed by a longer lived decay. Brorson *et al.* used the "Fermi level smearing" concept, borrowed from work on metals, to interpret their results. When the electron temperature is increased by the pump pulse, the tails of the Fermi distribution spread far out in energy, opening states below and filling states above the Fermi level. Depending on the probe wavelength and the position of the Fermi level, the optical transitions may be enhanced or blocked. Similar explanations were adopted by others [13, 36]. Kaindl has pointed out, however, that the stationary spectra show no sharp spectral features. In essence, if a smearing effect is acting, it is on a rather featureless surface, so this mechanism may not play a role in the photoinduced response.

By controlling temperature, Chwalek *et al.* first demonstrated that the changes in the photoinduced response were intimately linked with superconductivity [13]. They observed that cooling through the transition temperature increases amplitude of the response and increases the relaxation rate. These properties are not confined to YBCO, they appear to be a more general feature of the cuprates [23]. Just as we find in our own data, Chwalek's results show the amplitude of the response roughly tracks the temperature dependence of the superfluid density. In comparable nonsuperconducting samples, only small gradual changes were observed in amplitude of response and decay rate.

Han *et al.* were one of the first to offer a microscopic picture of the photoexcita-

tion process. In the first 500 femtoseconds, photoexcited carriers thermalize producing an avalanche of quasiparticles. This is followed by a recombination stage in which Cooper pairs reform. Assuming all the energy of the photon is absorbed and converted into excitations above the gap energy we could expect approximately 30 e-h pairs to be created per photon. Thermalization to the nodes could create even more excitations since the gap goes to zero.

In the same paper Han and coworkers also addressed the recombination kinetics in terms of the Rothwarf and Taylor equations [56]. The pair of coupled differential equations describes the interaction between quasiparticles and phonons and successfully explains the "bottleneck" effect observed in conventional superconductors. Recombination phonons created when quasiparticles traverse the gap, may create other quasiparticles. Thus recovery of the condensate is set by phonon (with $E>2\Delta$) dissipation, not the density of quasiparticles. Han *et al.* cite evidence for such a mechanism in optimally doped YBCO since the recombination rate does not appear to be very sensitive to laser fluence at 20K. We find this to be an incomplete analysis and discuss it in more detail later. We will also address the special considerations of recombination kinetics in *d*-wave materials later.

Coherent phonon effects in superconducting cuprates were first reported by Albrecht [1], and more recently by others [49]. An earlier report in nonsuperconducting samples can be found in reference [30]. The effect refers to the process whereby pumping with a femtosecond laser results in reflectivity changes which oscillate with a high spatial and temporal coherence. Mazin *et al.* [47] proposed that superconductivity induces small displacements in the equilibrium positions of the ions. Because the pairing energy depends on the density of states at the Fermi level, this changes the ionic positions. Destroying su-

perconductivity restores the normal equilibrium positions, exciting coherent phonons. We have never seen such oscillations possibly because our pulse width is not short enough.

Much of the recent published work on pump probe effects has come from the Mihailovic group. They have examined a number of different superconductors: YBCO [21, 36, 67], BSCCO [67], and $Hg_1Ba_2Ca_2Cu_3O_{8+\delta}$ [20]. They find no evidence for *d*-wave character gaps in any of the samples they study. This conclusion is based on a model which relates the reflectivity amplitude and relaxation time to gap magnitude, symmetry and temperature dependence. Flying in the face of an overwhelming body of evidence, Mihailovic *et al.* also find evidence for two simultaneous gaps in the optimally doped and overdoped region of YBCO and only one gap in the underdoped material.

Mihailovic has provided an analysis of the effects of laser heating in these types of experiments. There are two types of laser heating: transient and steady-state. Steady-state heating refers to the average temperature increase from a stream of pulses, while transient refers to the temperature increase from a single pulse. We have observed steady-state increases in temperature as evidenced by the temperature sweeps(see figure B.3). A detailed theoretical treatment is available in reference [19]. Whether measured or calculated, steady state increases can be significant ($\sim$10K).

An estimate of individual pulse heating may be determined using the heat capacity relation: $\Delta Q = v\rho c\Delta T$. Using the following parameters: single pulse: ΔQ=0.2nJ, mass density: ρ=6.4$\times$10$^{-3}\left[\frac{kg}{cm^3}\right]$, excitation volume: v= 7.9$\times$10^{-10}cm^{-3}, heat capacity: c=170$\left[\frac{J}{kgK}\right]$ we find the transient heating is $\sim$0.2K. This estimate is based on the maximum pump fluence, so this is an upperbound for transient heating and probably not an important con-

sideration. Decreasing the repetition rate of the laser using a pulse picker or similar device could mitigate the effects of steady-state heating, without diminishing the single pulse energy. A smaller increase in the steady state heating can also be achieved by using thin films. The superior thermal conductivity of a substrate such as $SrTiO_3$ or MgO will provide much better thermal anchoring and result in a closer correlation between the superconductor and the ambient temperature.

Using photothermal microscopy, Studenmund *et al.* studied temperature dependent effects on reflectivity [24, 65]. This technique measures the change in reflectivity due to heat diffusion from a focussed laser spot. Two 2μ diameter laser beams are separated by 10μ, one monitors the influence of the other. The result is a curve which shows a temperature dependence that peaks at T_c, figure 4.1. Polarized temperature-swept measurements in optimally doped YBCO (figure 4.2) show strikingly similar behavior. Thus we may be able to observe bolometric effects, but only in one instance. All other temperature dependences measured were characterized by much larger signals which continued to decrease through T_c.

Comparison with the results of Holcomb *et al.* [32, 34] is also informative. By measuring the sample's reflectance(0.3-4.5eV) at two temperatures, they also extract the thermal properties of the material's reflectance. Changes in reflectivity due exclusively to the onset of superconductivity may be observed using their experimental technique. Their results are shown in figure 4.3. Stevens [63] conducted pump-probe studies at a few different probe energies and find a rough wavelength correspondence with Holcomb's results. So in addition to monitoring the partial destruction and reformation of condensate, pump probe

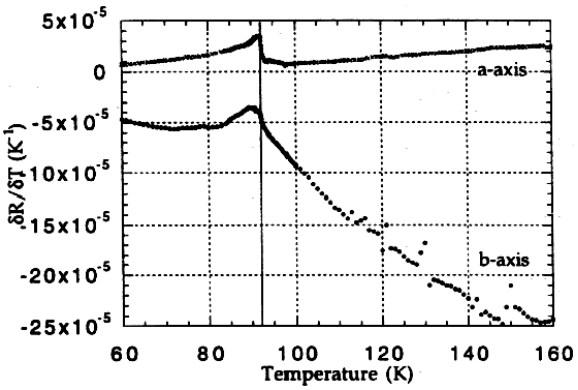

Figure 4.1: Results from [65] on optimal YBCO. This is not a femtosecond technique. Two beams, a pump(514nm) and probe(780nm) are separated by 5 beam diameters. Changes in reflectivity from thermal waves created by the pump beam are measured by the probe. Two different polarization directions are measured. Other probe energies produce temperature traces showing sharp discontinuities at T_c. Since nearly all pump probe studies find a qualitatively different temperature dependence from the one depicted here, we conclude that bolometric heating does not play a role in the picosecond response.

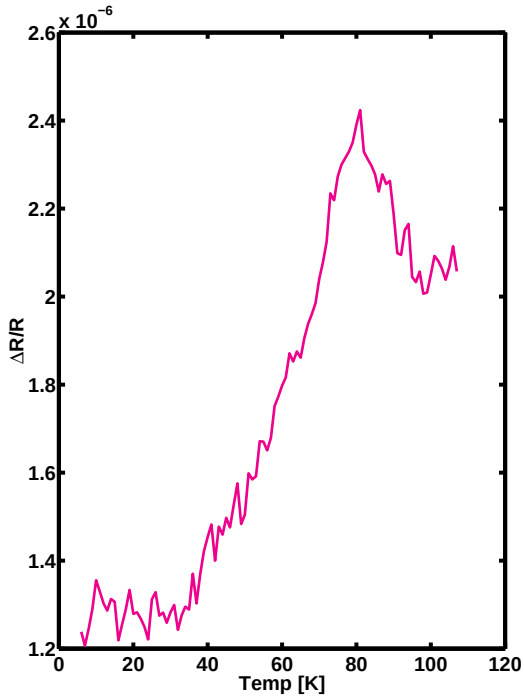

Figure 4.2: Optimal YBCO for pump and probe along a-axis. We discuss this result in more detail in chapter 6. See text for comparisons to figure 4.1

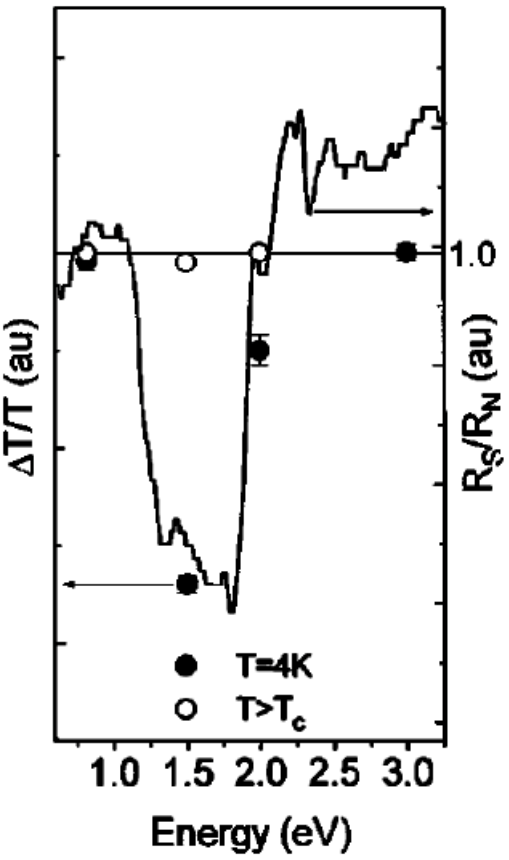

Figure 4.3: Pump probe comparison with thermal difference spectroscopy. The technique, described in reference [34], measures the temperature derivative of the optical reflectivity. The solid line is the ratio of the reflectivity of superconducting over normal YBCO (R_S/R_N). The solid circles are the amplitude of the response of degenerate pump probe spectroscopy measured at 4K (in transmission $\Delta T/T$). From reference [63].

effects measure changes between the superconducting and normal state without raising the sample above T_c. Holcomb's results will also be an important guide for future experiments which seek to explore the wavelength dependence of the picosecond response further.

Motivated by observation of large changes in infrared reflectivity upon cooling below T_c, Kaindl and coworkers carried out infrared pump probe measurements. The method is detailed in reference [37]. Figure 4.4 shows the picosecond lifetimes they observed agree well with previously published results at optical frequencies, despite more than an order of magnitude smaller probe energy.

Kaindl demonstrated a correlation between his ultrafast results and differential reflectance spectroscopy. He compares results in the probe range of 60-180meV with difference

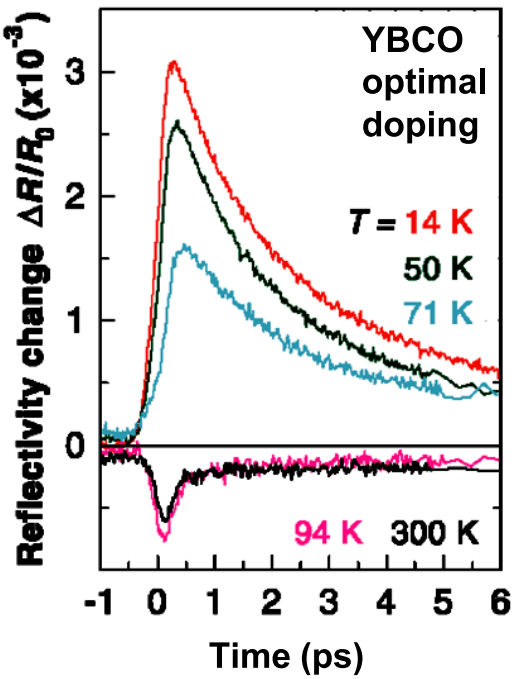

Figure 4.4: YBCO optimal film pumped at 1.6eV and probed 90meV. Note the amplitude of the effect is much larger than 1.5eV probe experiments. The lifetime, however, is the same. From reference [40].

reflectivity measurements. In similar fashion to Stevens' result, figure 4.5 shows the sign and amplitude of the response, when scaled, follow the stationary response. Furthermore, the shape of the spectral dependence is independent of the magnitude of the pump fluence. Thus there appears to be ample evidence for interpreting pump probe results as an electronic excitation process: Ultrafast spectrally resolved studies exhibit the same wavelength dependence that stationary studies do.

If we further develop this model we see that changing the pump fluence controls the fraction of Cooper pairs broken, without appreciably increasing the lattice temperature on a picosecond time scale. Significant heating effects are observable, but on longer timescales. For example, transient photoimpedance measurements have identified bolometric responses to be on the order of nanoseconds[43]. This is in reasonable agreement with the thermal diffusion time constant: $\tau = \frac{d^2 c}{\kappa}$. c-axis diffusion is the principle diffusion path, since

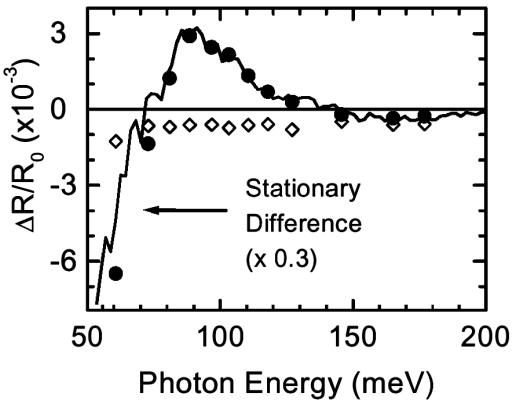

Figure 4.5: Solid line: Reflectivity measurements made at 95K were subtracted from a 20K scan. Solid dots: the amplitude of the picosecond response from pump probe experiments performed below at T=14K. Open diamonds amplitude of the picosecond response at 94K. [37]. Subtraction of the two sets of picosecond data produce a trace which is virtually identical to the solid line. This serves as further confirmation that pump probe techniques are sensitive to the presence of the superconducting state.

the smallest length scale, d, is the optical penetration depth, 1000Å. κ_c=.026$\left[\frac{W}{cmK}\right]$ is the thermal conductivity. The heat capacity at 80K is of order $1\left[\frac{J}{cm^3K}\right]$. With the above values we find a time scale of 4 nanoseconds.

Examination of the dependence of $\Delta R/R$ with pump fluence, would also suggest that bolometric effects play almost no role in the picosecond photoinduced response. Since superfluid density is not a linear function of temperature, increasing the pump would quickly lead to sublinear behavior as T_c is approached. Moreover we might expect a transition to such behavior to occur at lower and lower fluences as the cryostat temperature is set closer to T_c. As we shall see however, the response is linear over a large range of fluence, and this linearity is weakly a function of the ambient temperature of the sample.

Finally we briefly note other efforts to probe dynamics of superconductivity using various techniques. Feenstra and coworkers looked at dynamics on the microsecond timescale with a pump energy of 800cm^{-1} and probe energy of 5cm^{-1}. They attribute the 50 microsecond lifetimes they observe to bolometric heating of their sample. This is correlated with the expected temperature increase arising from the deposited energy of the pump

pulse. Relaxation time constants in the range of 5-25μsec are identified with quasiparticle recombination. Energetic considerations would dictate quasiparticles relax to the nodes. In this region, however, a clear picture of quasiparticle recombination process is stymied by theoretical considerations. The acoustic phonon dispersion and quasiparticle dispersion do not cross. In other words, energy and momentum cannot be simultaneously conserved. So a complete theoretical description of quasiparticle recombination awaits.

Using an optical pump and terahertz probe technique Siders *et al.* measured the complex conductivity, obtaining directly what we have inferred: a picture of the quasiparticle and superfluid dynamics [3, 60]. Temporal resolution was limited to one picosecond, about the period of THz radiation. They find the recovery dynamics for $YBa_2Cu_3O_{6.5}$ is considerably slower than for optimally doped YBCO, consistent with our observations. In all cases they observed that more than 20% of the superfluid did not recover after 20 picoseconds. Since they can easily convert their results to a superfluid density they can determine what fraction of the condensate is destroyed.

We can estimate the number of Cooper pairs destroyed. We first determine energy density using a pulse energy of .3nJ/pulse, a beam waist of 100μ, and a penetration depth of 1000Å. If we assume a photon breaks thirty pairs, 3×10^{10} quasiparticles are generated per pulse. The hole density is estimate to be approximately 1.8×10^{21} cm^{-3}. Thus we estimate 2% of the condensate is destroyed in our experiment.

For comparison, we estimate the number of thermally excited quasiparticles at a fixed temperature below T_c. Near the nodes, where the low energy excitations occur, the quasiparticle density of states is, from reference [46], $N(E) = \frac{2}{\pi\hbar^2}\frac{1}{v_F v_2}E$ where $v_F \sim$

2.5×10^7cm/s and v_2=v_F/19 are the quasiparticle velocity normal and parallel to the Fermi surface. Upon substitution of E with k_BT and integration of the density of states up to 10K, we find a quasiparticle density of 3×10^{17}cm^{-3}, much smaller than the photoexcited density. In spite of the quadratic temperature dependence, thermal quasiparticles contribute little to the total density at T_c.

In this chapter we have provided an overview of the important advances in pump probe spectroscopy to date. We have tried to emphasize a particular interpretation of the photoexcitation process. Pump probe spectroscopy measures conversion of condensate into quasiparticles via an electronic mechanism. Recovery of the condensate occurs within a few picoseconds. In this picture, the risetime of the response is assigned to the rapid thermalization of electrons to the lowest lying states above the gap. Energetic arguments favor a relaxation of quasiparticles to the nodes, with the penultimate step as yet unresolved. Bolometric mechanisms are expected to play a role on nanosecond timescales and are not seen to play a central role in the ultrafast pump probe response.

Chapter 5

$Bi_2Sr_2CaCu_2O_{8+\delta}$ and the Nodal Quasiparticle Picture

$Bi_2Sr_2CaCu_2O_{8+\delta}$(BSCCO) was the first system we studied. Our findings on the temperature and intensity dependence are consistent with the $d-$wave character of the superconductor. These data also provide a useful backdrop for the subsequent discussion of YBCO.

BSCCO thin films are grown on $LaAlO_3$ substrates using atomic layer-by-layer molecular beam epitaxy [22]. Fine control of the film growth is achieved by depositing constituent layers one at a time. Five layers of BSCCO(2201) are deposited before 40-60 layers of BSCCO(2212) are grown. It is the response of these layers that we discuss below. The transition temperature is 85K.

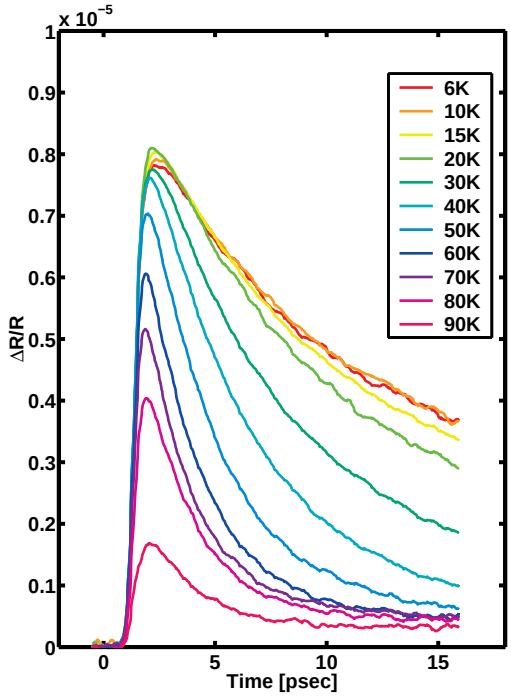

Figure 5.1: Optimally doped BSCCO: The photoinduced response as a function of time for a range of temperatures. The pump intensity is held constant $\sim$ 25mW

5.1 Temperature and Intensity Dependence

Figure 5.1 shows the temporal response in optimally doped BSCCO for a fixed pump intensity. As the temperature increases the amplitude of the response falls. In addition the decay rate increases up to about 50K.

In Figure 5.2, the roles of temperature and intensity are exchanged. With the temperature held constant, we examine the effect of pump intensity on recombination rate. The normalized traces show clearly the increase in lifetime as the pump intensity is decreased by nearly a factor of ten. Note: all our data plotted in this thesis have a time axis which is relative, not absolute. An absolute measurement of zero time delay can be obtained by

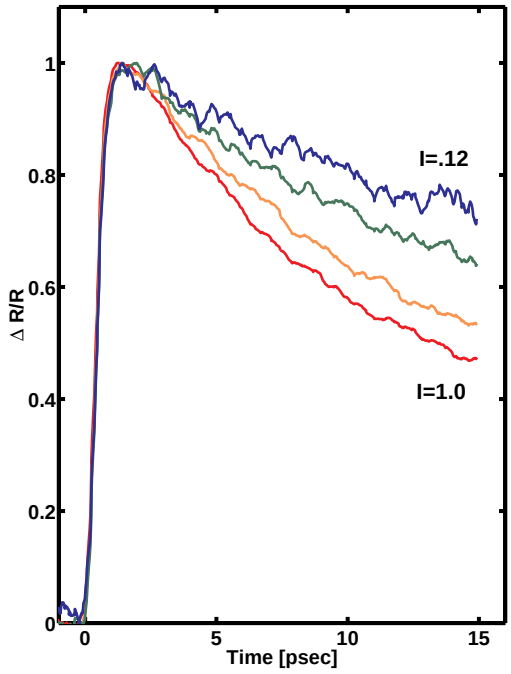

Figure 5.2: BSCCO response plotted *vs* time, normalized to show the variation in decay. Pump intensities are normalized too, and are shown for: 1.0, 0.54, 0.24, 0.12.

performing an autocorrelation measurement with a doubling crystal.

Figure 5.3 serves as a check that higher intensity pulses do not mix in nonlinearities. For higher fluences, sublinear behavior has been observed in the peak response of the pulse [37], probably reflecting a saturation of the signal because the maximum number of quasiparticles have been created. Exploring saturation behavior may be useful for determining an upper bound for the fraction of the condensate depleted.

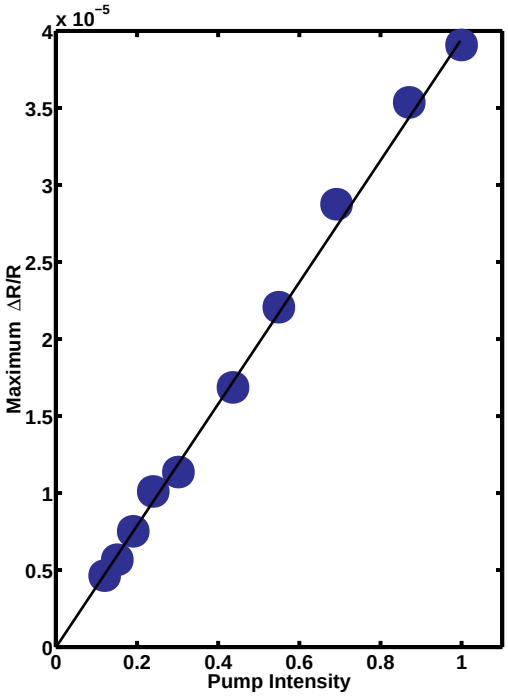

Figure 5.3: Peak amplitude of the response *vs* pump intensity. The maximum pump power was $\sim$ 25mW and the probe was $\sim$ 3mW. The actual power incident on the sample is somewhat lower since there are 3 cryostat windows that the beam must traverse. It is worthwhile considering what occurs when the ratio of pump and probe beams approaches unity. This can be understood by stressing that the probe beam always depletes condensate at all time delays. Provided that the probe beam is weak, it lowers the maximum superfluid density only slightly. Thus the pump beam acts to modulate the maximum superfluid density set by the probe.

5.2 Analysis of Decay Rate

A primary goal of this pump probe work is explication of the kinetics of decay, and curve-fitting the time dependences is a natural path towards elucidating the underlying physics. By plotting figure 5.1 on a semilog axis (figure B.1) we find that BSCCO's response is dominated by a single exponential decay. This simple character makes a dynamics analysis seem tractable.

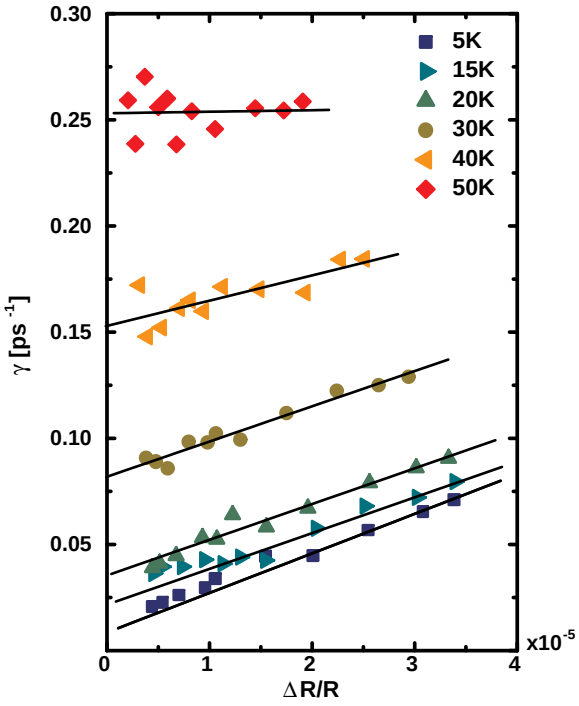

Figure 5.4: BSCCO: The extracted decay rate plotted *vs* ΔR/R.

Rather than attempting to fit the entire time trace, we choose to focus on the recombination rate which reflects the recovery of the condensate only. Thus we adopt a simplified approach to extract the decay rate of interest. We perform a single exponential fit to the decay in the period between 2-7 picoseconds. The influence of any fast transient process as well as very long time scale behavior [48] is thus minimized. Such a method is well defined and captures the central dynamical effect: the decay rate changes dramatically at T_c [13]. Figures 5.1 and 5.2 may be compactly summarized in figure 5.4. The decay rate increases linearly with pump intensity, while the effect of temperature is to increase the decay rate even more rapidly. A scaling analysis of the data shows that best collapse of decay rates occurs when plotted against $T^2+\eta\Delta$R/R. Such a collapse is naturally motivated

in the context of nodal quasiparticles described in the next section.

5.3 Nodal Quasiparticle Density of States

An important consequence of the gap structure of d-wave superconductors is the presence of zero energy excitations at the nodes. These nodal quasiparticles give rise to a linear T dependence of the superfluid density and a T^2 dependence of the heat capacity [50]. Such properties may be calculated once the shape of the density of states is known. Modifying the BCS model to incorporate the angular dependence in the gap magnitude reproduces the correct form for the density of states [45]. From such an analysis we find the density of states near the node is linear in energy [12]. Moreover, the total number of quasiparticles up to an energy E, is proportional to E^2. This is illustrated in figure 5.6.

By recasting figure 5.4 into figure 5.5 we combine the effects of temperature and intensity. In this form, we emphasize that either parameter may determine the recombination rate. Whichever term dominates the quasiparticle density determines the dynamics. As the density of electrons and holes increases, the probability per unit time that any pair recombines also increases. This is in contrast to the conventional superconductor picture where the recombination process is limited by "bottleneck" effect previously described. The quasiparticle population has two sources: thermal and photoexcited. Because of the quadratic dependence of the rate on temperature, the thermal contribution appears linked to the nodal quasiparticle density of states picture. Temperature serves the role of the characteristic energy described above.

In this chapter we have argued that the recombination rate reflects the quasipar-

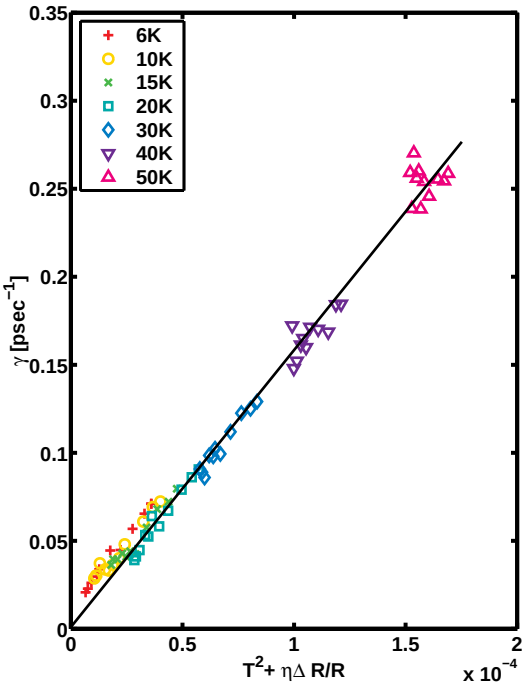

Figure 5.5: The extracted recombination rate is plotted *vs* $T^2+\eta\Delta R/R$. η is an empirically determined proportionality constant which relates the 0-temperature recombination rate to the photoexcitation density. Same data as figure 5.2.

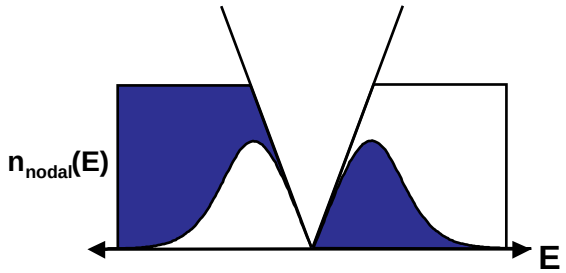

Figure 5.6: Schematic of *d*-wave density of states. Blue shows electrons in thermalized distributions.

ticle population. This population has two components, one thermal and one photoexcited. The quadratic dependence of the thermal component is consistent with the nodal quasiparticle density of states picture; the number of excitations is expected to vary as E^2.

Chapter 6

$YBa_2Cu_2O_x$

By comparison to BSCCO we have studied $YBa_2Cu_3O_x$ (YBCO) much more extensively. We studied untwinned single crystals with two levels of doping: $O_{6.5}$ (underdoped T_c=58K)and $O_{6.993}$ (optimal T_c=93K). From these two crystals, an amazing range of complex behavior has emerged.

In the last ten years much progress has been made in improving the quality of these samples. The synthesis techniques are described in reference [41, 42]. The crystals we have studied are exceptional in their purity. As grown, however, they are twinned. By applying a uniaxial stress during a post-growth anneal the sample can be detwinned. Obtaining a detwinned crystal is thus a delicate process with low yield. Because these samples are single domain we are can measure the photoinduced response along the principal axes of the crystal.

6.1 Temperature and Intensity Dependence of Two Dopings

The underdoped phase we study is known as Ortho(rhombic) II phase. It is a highly ordered phase in which oxygen sites are fully occupied and completely vacant on alternating chains.[1] From the picosecond perspective, underdoped YBCO appears similar to BSCCO in that the lifetime increases dramatically at the lowest temperatures. It also has the familiar pump intensity dependence: recombination rate increases with pump fluence.

Much of the early work on the recombination rate focussed on the transition near T_c[23, 29, 30]. Little attention was paid to the behavior at low T. This is in part due to the focus on optimally doped YBCO, where little change in the recombination rate in optimal YBCO is observed. The dramatic differences in quasiparticle kinetics for two different dopings is one of the major findings of this research effort. Figures 6.1 and 6.2 show the effects just described.

Anisotropy in the linear optical properties was studied some time ago [58]. Only recently has there been one brief report of anisotropy in the ultrafast properties [62]. We provide the first careful, comparative study of the strong anisotropic behavior in optimal and underdoped YBCO. Figures 6.3, and 6.4 show remarkable differences between the samples. Whereas the underdoped sample appears to have a response which differs only in amplitude, the optimal sample *aa* direction is quite a surprise. Its decay kinetics are nothing like the *bb* direction, and are smaller by a factor of five.

[1] At high temperature, $O_{6.5}$ stoichiometry is tetragonal, oxygens are randomly scattered. As the sample is cooled, an Ortho I phase appears with chains running in perpendicular directions. This is the source of twinning. Below about 400K, the Ortho II phase becomes thermodynamically stable. A truly ordered phase is only realized with the application of uniaxial stress, otherwise mixed phases may occur. For highly ordered systems three phases are possible, Ortho I (nearly optimal) T_c=90K, Ortho III T_c=75K has two full chains followed by one chain empty, and Ortho II T_c=60K.

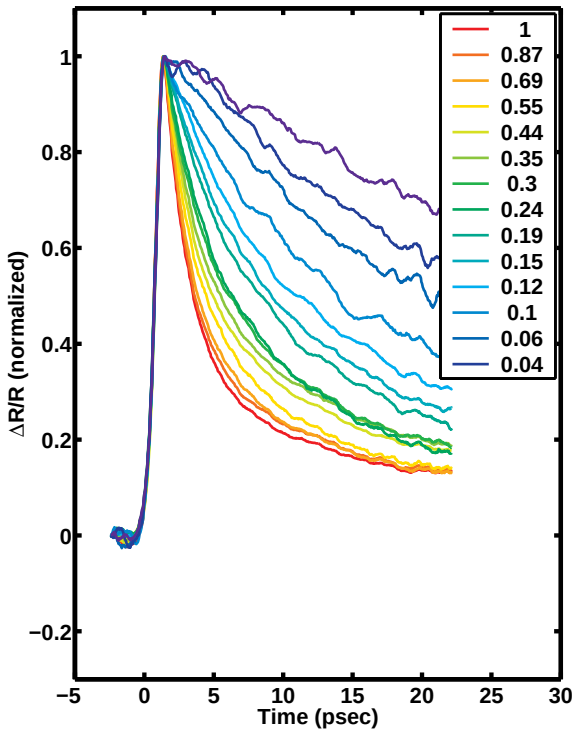

Figure 6.1: Underdoped YBCO: Normalized time traces showing that lifetimes are sensitive to pump intensities at low temperatures. At ∼30K the intensity dependence fades out. The dynamics are quite similar regardless of polarization direction. T=10K.

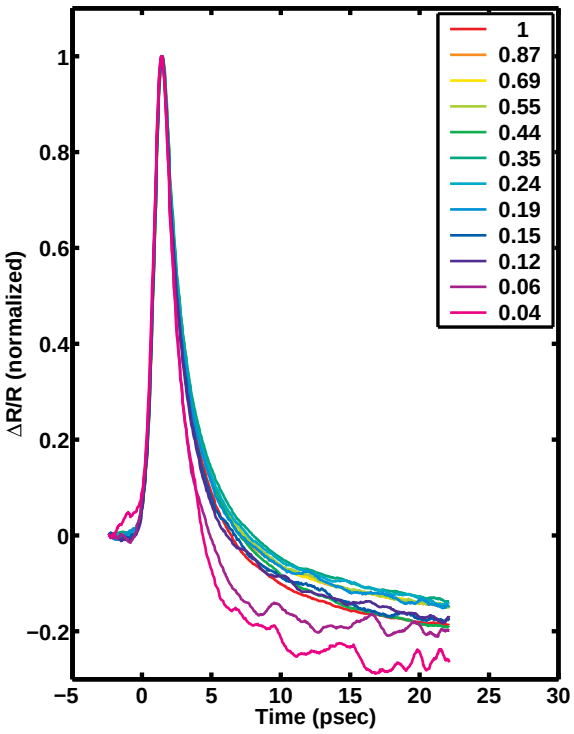

Figure 6.2: Optimal YBCO: The traces have been normalized to show that the recombination lifetime is insensitive to pump fluence. T=10K. Polarization configuration is *bb*.

We now limit the discussion to the two parallel pump-probe configurations. Plotted in Figure 6.5 is a temperature-swept scan where only the peak amplitude of the response has been recorded. Surprisingly the amplitude of the planes-only direction is small and relatively insensitive to temperature. It is slightly peaked near T_c. A peaked response character has been explained previously using a coherent phonon approach [47]. In the next chapter, we show that the $a-$axis demonstrates other unusual properties when in an externally applied magnetic field.

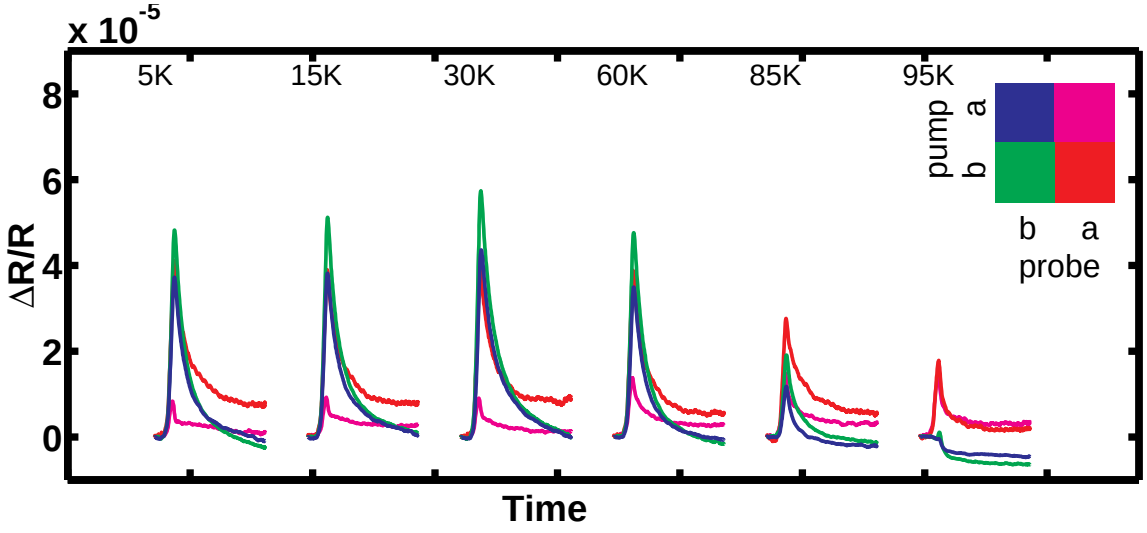

Figure 6.3: Optimal YBCO: Temporal response for various temperatures and fixed pump fluence. The four possible polarization configurations that can be measured are perpendicular (a-) and parallel (b-) to the chains for the pump beam and similarly for the probe beam. Comparing the red and magenta traces to the blue and green ones, we see the probe beam is far more influential than the pump beam in determining the shape of the photoinduced response.

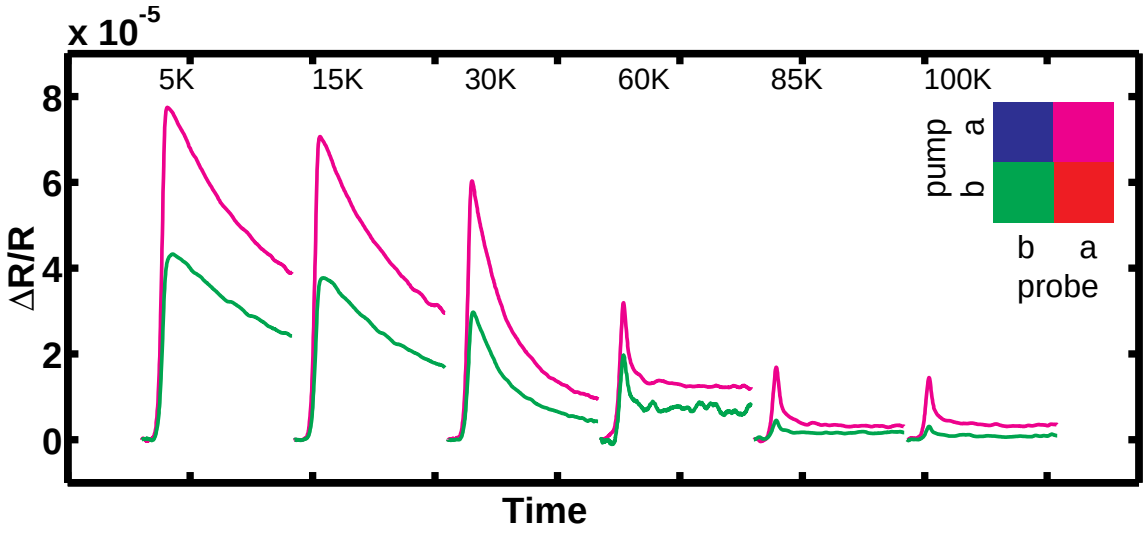

Figure 6.4: Underdoped YBCO: Two of the four polarization directions are shown, approximately the same pump fluence as in 6.3. Apparently the aa axis has two times greater signal than bb, in contrast to optimal which is smaller by a factor of 5. Subsequent measurements have shown that the shape of the traces change smoothly at 60K. All traces are 20psec.

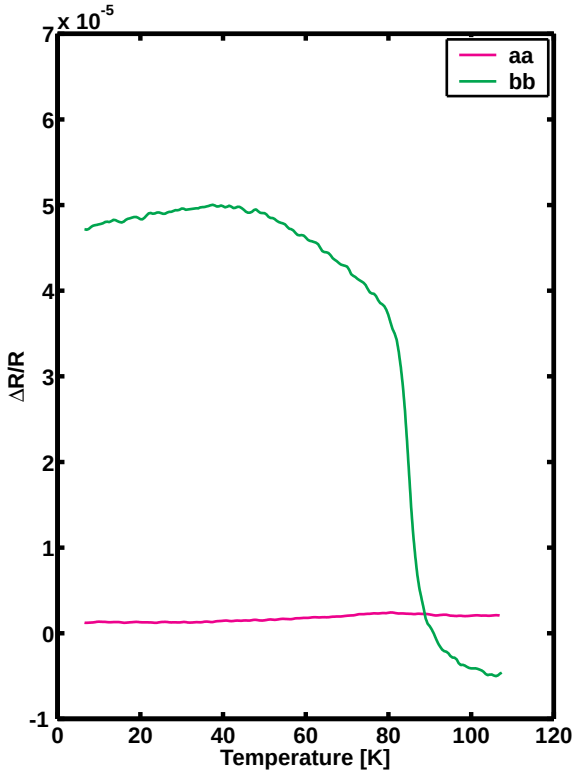

Figure 6.5: Optimal YBCO: The peak response is plotted *vs* temperature for the highest pump fluence. A pronounced anisotropy is apparent in optimally doped YBCO.

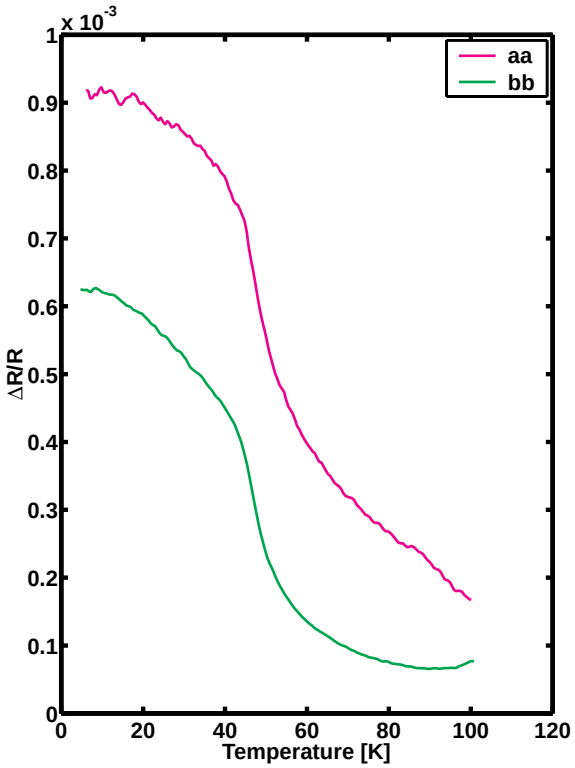

Figure 6.6: Underdoped YBCO: The peak response is plotted *vs* temperature. Compared to optimal, the difference in the signal amplitude is due to a difference in pump fluence. The intrinsic response is the same order of magnitude in each material.

Chapter 7

Magnetic Field Effects

That magnetism is the key to superconductivity is a mantra oft repeated by many practitioners in the field. To that end, we report on the influence of magnetic field on ultrafast dynamics in cuprates for the first time. Fortunately some experimental and theoretical work have already suggested a link between optical measurements and spin excitations. Leading the experimental side, Kaindl first demonstrated evidence for a link between ultrafast photoinduced response and recent inelastic neutron scattering data. We preface discussion of our results with a summary of the findings of neutron scattering, and a review picosecond data in the infrared.

7.1 Neutron Scattering and the Picosecond Response

As previously mentioned in chapter 3, hole doping into the CuO_2 planes destroys the long-range AF-ordered phase. This raises the fundamental question of the role of magnetism in the superconductivity mechanism. Inelastic neutron scattering has taken center

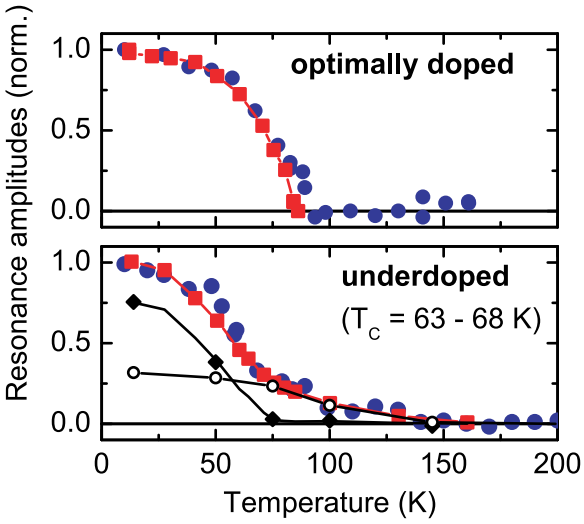

Figure 7.1: Picosecond data compared with neutron scattering. Red circles are peak response of photoinduced reflectivity measured at 90meV. Blue circles are 41meV neutron scattering data from [18]. Curves are normalized at 15K. The two black lines are obtained from a single value decomposition showing how the response can be constructed from two components one associated with T* and another with T_c.

stage as it has revealed the presence of short-range AF spin correlations at all doping levels. In YBCO, spin excitations extend over several hundred meV, but are confined around the (π, π) direction in momentum space. In the transition to the superconducting state, a peak emerges out of the broad background, at ∼40meV for optimal doping, ∼34meV for $YBa_2Cu_3O_{6.6}$. The discovery of this resonance peak has been the genesis of a number theoretical descriptions that incorporate antiferromagnetic interactions. Some view this effect as a readjustment in spectral weight within the spin excitation spectrum. The spectral weight comes from energies below 2Δ. This resonance appears at all doping levels for two classes of cuprates, BSCCO [26] and YBCO and is absent in $La_{2-x}Sr_xCuO_4$.

Evidence for a link with the photoinduced reflectivity is made clear in Kaindl's analysis. Figure 7.1 compares the amplitude of infrared picosecond data with the strength of the resonance. The virtually identical temperature dependence is remarkable. To explain

this result, Kaindl draws on recent theoretical work [11, 51, 52] that argues conducting carriers strongly couple to the 41meV spin fluctuations. The fact that this work compares *stationary* optical properties with the neutron data should pose little difficulty since we have already shown (figure 4.3) evidence that the spectral character femtosecond data agrees well with the stationary response.

Femtosecond spectroscopic data was collected by pumping and angle tuning a GaSe crystal [38], a material exhibiting a large nonlinearity. Single value decomposition was then used to reduce the data set. Loosely speaking, the analytical method determines the basis vectors which span the data. In other words, the numerical technique determines how many exponential decays should be used to construct each time trace. More on the analytical technique can be found in reference [54]. The result in figure 7.1 on underdoped YBCO shows two timescales describe the data completely. The slow component ($\sim$5psec) goes to zero at T_c, and is associated with the condensate. The fast component ($\sim$700fsec) disappears at the pseudogap temperature, T*, and is associated with some other type of correlated carriers. This important result highlights a general feature of the ultrafast technique which is not available using traditional spectroscopy methods. Exploiting the time domain, it is possible to separate multiple contributions to the reflectivity at a given frequency by distinguishing between different relaxation dynamics.

7.2 Neutron Scattering in a Field

To date, there are only two published reports on the effects of magnetic field on the amplitude of neutron resonance. The first paper is a brief report by Bourges *et al.* [8]

on optimal YBCO. On applying an 11.5T field in the *ab* plane, they find only the resonance linewidth changes, slightly increasing. Recently, Dai *et al.* [17] applied a field in the *ab*-plane on underdoped YBCO. They find that the peak amplitude is suppressed by about 10%. Imposition of a 6.8T field along the *c*-axis shows a more dramatic depression in the signal: about 30% (figure 7.2).

Consideration of the possibly relevant energy scales shows just how remarkable this result is: The upper critical field is much larger than the one applied: B_{c2} is 45T. The Zeeman energy, $\sim$ 0.8meV assuming g=2 and S=1, is much smaller than the resonance or thermal energy, $k_b T_c \sim$ 6meV. Thus the usual suspects appear to be counted out for the time being.

The possible significance of the response to the magnetic field has been addressed by Dai and others [35]. They have previously stressed that the temperature and doping dependence of the resonance is intimately connected to the electronic part of the specific heat. They find further support for the correlation in the magnetic field result [17].

Not mentioned in the literature is the possibility that this is a manifestation of the reduction in the condensate density. If so, we would expect it to have an $\sqrt{H}$ dependence. Little change with B $\parallel$ *ab* plane suggests that the 2-dimensional orbital component of the superconductivity is more significant than spin interactions.

7.3 Picosecond Response in a Field

We now revisit the notion that the principle component of the photoinduced response involves the condensate. The magnetic field response, however, does little to clarify

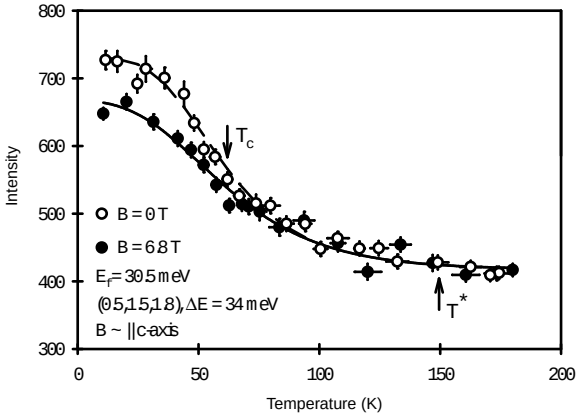

Figure 7.2: Underdoped YBCO: Temperature and field dependence of the neutron resonance from [17].

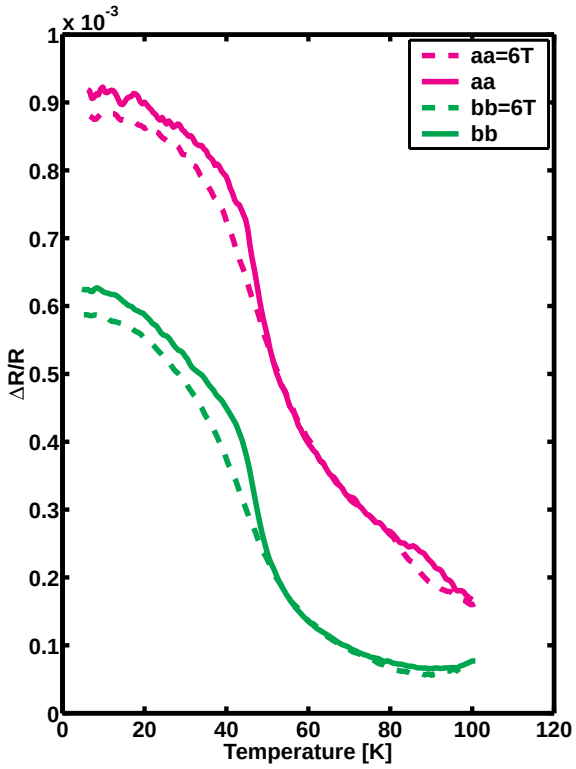

Figure 7.3: In underdoped, a 6T field depresses the amplitude of the response for both directions. Note there is no field effect in the pseudogap.

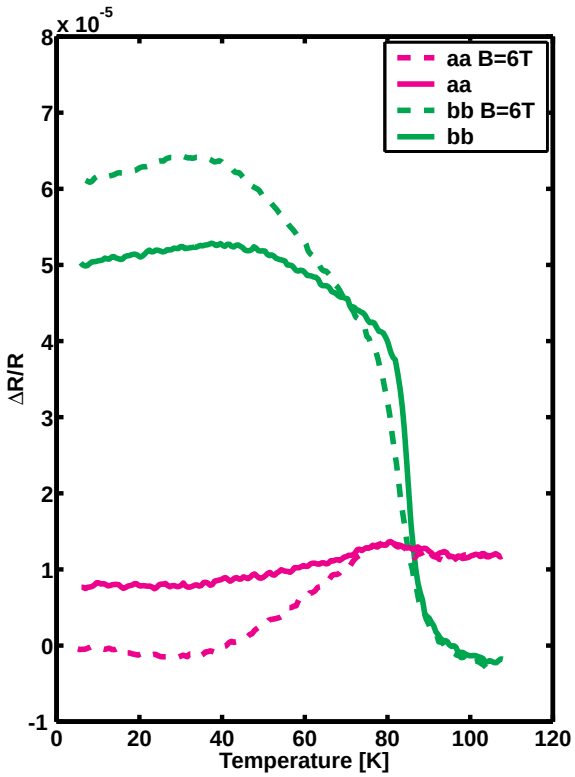

Figure 7.4: Optimal YBCO: A 6T field induces large changes in optimal than in underdoped. The behavior is also more complex, with an enhancement occurring parallel to the chains, and depression perpendicular.

the relationship between superconductivity and photoexcitation. We offer a few cursory observations: Figure 7.3 shows that 6T field depresses the underdoped response, while figure 7.4 shows the optimal response split: depressed perpendicular to the planes, and enhanced parallel. Clearly the response and the condensate are not related in a simple fashion. A spectral resolved study may provide answers to some of these questions. The underdoped evidence shows clearly that the pseudogap is not sensitive to the magnetic field. This may be a toehold for future theoretical efforts.

The link between pump probe spectroscopy and neutron scattering has already been forged. Our analysis is presently bound by the limited neutron data: In qualitative agreement with scattering results, we see an enhancement in optimal and a depression in underdoped. If a straightforward relation with neutron scattering could be established, practitioners of ultrafast physics would have an advantage: the superior signal to noise ratio this technique offers. In determining whether spin excitation physics is reflected in ultrafast experiments ought to be a priority of future experimental efforts.

We now address the change of dynamics in a field. Figure 7.5 presents another curious result that awaits explanation. The b-axis response shows a slight increase of lifetime in the magnetic field. Dramatic changes, however, occur along the a-axis. The picosecond decay so typical of these materials was found to be absent in 0 field measurements. It is apparently generated (or recovered) in the presence of the magnetic field. Moreover, it has a familiar qualitative temperature dependence, namely the decay rate increases as the temperature rises.

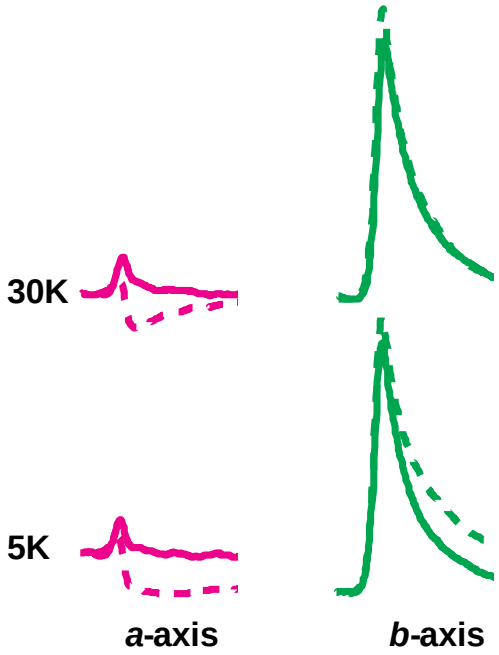

Figure 7.5: Optimal YBCO: As before, magenta and green correspond to a-and b- respectively. Dashed lines indicate 6T field.

Chapter 8

Theoretical Models

In this chapter we speculate on a few of the important issues central to understanding the nature of pump probe spectroscopy.

8.1 Two-Fluid Model and Optical Frequency Response

One of challenges posed in the introduction is to explain how a probe can be sensitive to transformations occurring at the energy scale of the gap, yet be far removed in energy. One answer rests with the application of the two-fluid model. As its name suggests, the model allows us to approximate properties of a superconductor by considering the two contributions of quasiparticles and condensate to the electrodynamic properties. The two expressions below follow from the Drude model and a full discussion can be found in [68].

Using this framework, we first calculate the complex conductivity, $\sigma \equiv \sigma_s + \sigma_n = \sigma_1 + i\sigma_2$ where σ_s is the contribution from the condensate, and σ_n is the quasiparticle component.

$$\sigma_s(\omega) = \frac{n_s e^2}{m}\left(\frac{\pi}{2}\,\delta(\omega) + \frac{i}{\omega}\right) \tag{8.1}$$

$$\sigma_n(\omega) = \frac{n_n e^2}{m}\frac{1}{1/\tau - i\omega} \tag{8.2}$$

τ is the quasiparticle scattering time. Equations 8.1 and 8.2 are linked by a conductivity sum rule. It dictates that spectral weight (or the total number of carriers, $n_s + n_n$) must always be conserved. It is often expressed in the following form:

$$\int_0^\infty \sigma_1(\omega)\, d\omega = \frac{\pi n e^2}{2m}. \tag{8.3}$$

Therefore when the photoexcitation process depletes the superfluid δ-function, real quasiparticle conductivity must increase correspondingly. We are however free to determine how it is to be distributed, provided that our distribution has some physical basis. Empirical reflectivity data [57] of σ_1 show that spectral weight is lost up to about 1000cm^{-1} upon cooling, but it is most strongly depressed at $\sim$400cm^{-1}.

The next step is to introduce the complex conductivity into a model of the linear optical properties. To fix on an example, we choose to model the optical properties along the *b*-axis of optimally doped YBCO. The linear optical properties are well characterized in the literature, and it is also the orientation for which we get the largest response (see figure 6.3). We simulate the complex frequency dependent dielectric function and use it to compute the reflectivity. The procedure is summarized mathematically as follows:

$$\tilde{\epsilon}(\omega) = \epsilon_\infty + i\frac{\sigma(\omega)}{\omega} \tag{8.4}$$

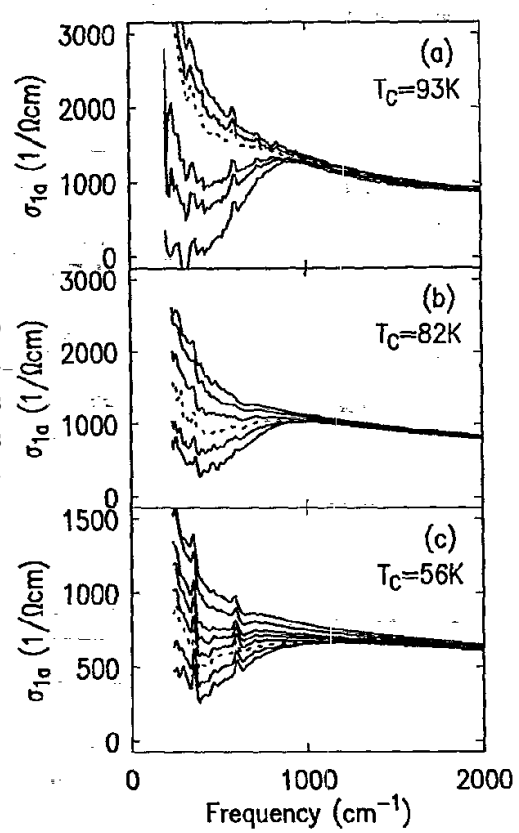

Figure 8.1: σ_1 measured for three YBCO single crystals for different doping levels. We note that these measurements are along the a-axis. The top figure shows optimal doping with the strongest depression at 400cm^{-1}. From reference [57].

$$R(\omega) = \left[\left|\frac{\sqrt{\tilde{\epsilon}(\omega)} - 1}{\sqrt{\tilde{\epsilon}(\omega)} + 1}\right|\right]^2 \tag{8.5}$$

We used the following parameters in modeling the complex conductivity: τ = 40psec, ϵ_∞=2(1+i), $\sigma_s + \sigma_n = 1.2\times10^7$[Ω-m]$^{-1}$. Such values may be extracted from [15, 45]. Checks can be made that the calculated penetration depth and the dielectric function behavior in our simulation agree well with empirical data.

We modify equation 8.2 to shift the spectral weight to a finite frequency (400cm^{-1}): $\omega \rightarrow \omega - \omega_o$. The two traces in figure 8.2 show the dramatic changes possible simply by shifting spectral weight at very low energies. At our probe energy, 1.5eV, the response is transformed from being small of the wrong sign to a response of reasonable magnitude with proper sign. In sum we present a scenario, using the two-fluid model, which shows how

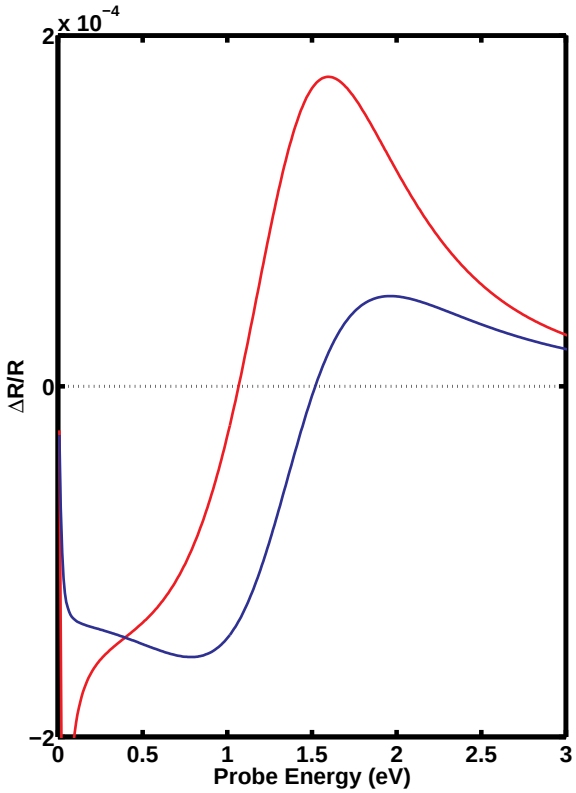

Figure 8.2: Two-fluid model simulation, using optimal YBCO *b*-axis optical properties. The fractional change in reflectivity resulting when 1% of the condensate is converted to quasiparticles. Red trace is shifted spectral weight response. Blue trace is unshifted spectral weight response.

the physics at gap energies can influence the visible frequency optical response. A more sophisticated model would shift the spectral weight to a band of frequencies. Spectrally resolved measurements would suggest further refinements to this simulation.

8.2 Recombination Mechanisms

The range of decay timescales observed leaves little doubt that a number of relaxation mechanisms are operating at any given time. As a departure point for analysis, we can model the recombination processes as a single exponential and a bimolecular process.

The differential equation which describes both processes is given by:

$$\frac{dn}{dt} = -\frac{n}{\tau} - \beta n^2 \tag{8.6}$$

The solution is:

$$n(t) = \frac{n_o e^{-\frac{t}{\tau}}}{1 + \beta\tau n_o(1 - e^{-\frac{t}{\tau}})} \tag{8.7}$$

Which term dominates the recovery process is determined by the rate limiting step. The bimolecular term ($\sim n^2$) describes a recovery in which the quasiparticle and hole must find each other to recombine. Such a mechanism is clearly photoexcitation density dependent. If quasiparticle and hole diffusion are sufficiently rapid their recombination may be limited by some other undetermined process. Whatever the pentultimate step, a reasonable assumption is that this occurs with finite and fixed probability per unit time meaning we should observe an exponential time dependence. A review of figures 6.1 and 6.2 suggest that underdoped YBCO appears to have an intensity dependence that may be consistent with the bimolecular picture, whereas optimal does not.

We argued previously that a recombination of a single quasiparticle with a hole via phonon emission appears to violate simultaneous conservation of momentum and energy. Thus higher-order processes seem worthy of investigation. As an example, one theoretical treatment has argued that quasiparticle-quasiparticle umklapp scattering processes predict the temperature dependence of the electrical transport properties [71]. How such processes can be translated into an analysis of time dependence is the task of future theoretical efforts.

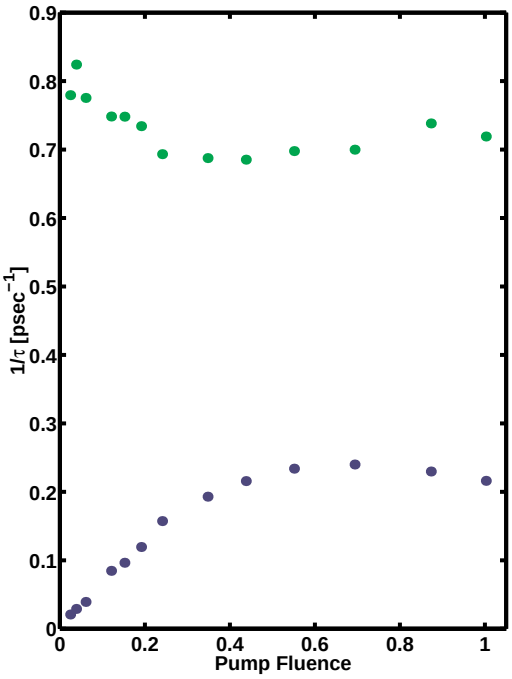

Figure 8.3: Decay rate *vs* pump fluence for optimal(green) and underdoped(blue) YBCO with pump and probe along *b*-axis. Rates are determined by fitting the data to a single exponential. The time interval fit was between 95% and 70% of the maximum. T=10K.

Chapter 9

Summary and Future Directions

We close by highlighting some of the central observations presented in this thesis.

Our research program has three principal aims: We wish to understand the recombination pathway following photoexcitation. We have made headway with an analysis of decay rates in a BSCCO film. Nodal quasiparticle recombination is likely the final step in the recombination process. Quasiparticle-quasiparticle scattering may also play an important role in the recovery of the condensate. A closely related issue we have carefully explored is the recombination dynamics. The lifetime spans well over an order of magnitude and has been studied as a function temperature, pump fluence, and magnetic field. As a general rule, recovery of the condensate slows with lower pump fluence or lower temperature. A final motivation has been to explain the sensitivity of the probe to low energy phenomena. The two-fluid model holds promise as an answer to that question.

In the course of our investigation we have encountered a number of interesting sample specific phenomena. An interesting result that should be further examined is the *aa*

axis response optimal doped YBCO. It is unusual because it apparently lacks the behavior we have come to associate with pair breaking. In particular, the response is extremely small and rapid. With the application of a magnetic field the familiar behavior is restored. Perhaps such response is unique to this probe energy.

A comparative study across classes of cuprates would be interesting. The nodal quasiparticle picture does not fit the YBCO data well. Understanding why this is so might be a big contribution to the field. Contrasts between dopings also merit a careful theoretical treatment. Notable is the pronounced sensitivity of recombination rate to pump fluence in underdoped below 30K. The variation in amplitude of response in a magnetic field also invites a physical description.

Beyond the necessary theoretical development we ultimately require, there are number of experimental avenues of interest: Developing spectroscopic capability is perhaps the most promising direction to pursue. As previously mentioned, this could provide a robust test of the two-fluid model's applicability to explaining the photoinduced response. Ultimately we would like to dramatically improve upon figure 4.3. A recent report on continuum generation(400-1400nm) in tapered fiber [6] holds tremendous promise. It appears easy to implement and could enormously enhance our understanding of the pump-probe response.

More magnetic field work could also prove interesting, especially if it can firmly establish a relationship with neutron scattering results. Progress might be made in clarifying the role of spin fluctuations in driving superconductivity. This scenario is particularly attractive since pump-probe data are more readily obtained with superior signal to noise

than neutron scattering data. Single value decomposition analysis might provide a picture similar to figure 7.1 showing that only the superfluid response is depressed below T_c in a field.

MgB_2 was very recently determined to be a superconductor at ~40K. Isotope shifts in T_c suggest that it exhibits the familiar BCS phonon-mediated type coupling. Nevertheless, little is known about the system at present and it may be instructive to probe its picosecond dynamics. If nothing else, its high T_c makes an examination of conventional superconductors more accessible. Buckyballs have also been studied and may be fertile ground to explore further [25].

A thorough analysis would have to establish the fraction of the response which is bolometric in origin. Looking along the *aa* direction in optimally doped YBCO at lower pump intensities while performing a temperature sweep, may sharpen the feature observed at T_c(figure4.2). Following the work of Studenmund, a similar experiment could be performed on the ultrafast system, again the pump and probe beams are displaced by at least a beam diameter.

This thesis has focussed on dynamics in the picosecond regime. There are, however, effects on much longer time scales which we did not address. Excised from the time traces presented is a DC offset. Preliminary measurements show that this offset scales with the average pump power and is also temperature dependent. A complete study must include an analysis of what interaction may exist between the amplitude of the offset and the picosecond dynamics. By introducing a pulse picker, it is possible to preserve the energy per pulse and decrease average fluence thus minimizing the DC offset.

Regardless which path is followed, patience is in order, if history is any guide. BCS theory explained superconductivity 42 years after Onnes' discovery. Only 15 years have elapsed since we embarked on the high-T_c odyssey.

Bibliography

[1] W. Albrecht, T. Kruse, and H. Kurz. Time-resolved observation of coherent phonons in superconducting $YBa_2Cu_3O_{7-\delta}$ thin films. *Physical Review Letters*, 69(9):1451–4, 1992.

[2] N. P. Armitage, D. H. Lu, D. L. Feng, C. Kim, A. Damascelli, K. M. Shen, F. Ronning, Z.-X. Shen, Y. Onose, Y. Taguchi, and Y. Tokura. Superconducting gap anisotropy in $Nd_{1.85}Ce_{.15}CuO_4$: Results from photoemission. *Physical Review Letters*, 86(6):1126–1129, 2001.

[3] R. D. Averitt, G. Rodriguez, A. I. Lobad, J. L. W. Siders, S. A. Trugman, and A. J. Taylor. Nonequilibrium superconductivity and quasiparticle dynamics in $Y_2Ba_3Cu0_{7-\delta}$. *Physical Review B (Condensed Matter)*, 63:140502 1–4, 2001.

[4] R. D. Averitt, G. Rodriguez, A. I. Lobad, and A. J. Taylor. Conductivity artifacts in optical-pump thz-probe measurements of $YBa_2Cu_3O_7$. *Journal of the Optical Society of America B (Optical Physics)*, 17(2):327–31, 2000.

[5] D. N. Basov, R. Liang, D. A. Bonn, W. N. Hardy, B. Dabrowski, M. Quijada, D. B. Tanner, J. P. Rice, D. M. Ginsberg, and T. Timusk. In-plane anisotropy of the penetration depth in $YBa_2Cu_3O_{7-x}$ and $YBa_2Cu_4O_8$ superconductors. *Physical Review Letters*, 74(4):598–601, 1995.

[6] T. A. Birks, W. J. Wadsworth, and P. S. J. Russell. Supercontinuum generation in tapered fibers. *Optics Letters*, 25(19):1415–17, 2000.

[7] D. A. Bonn, P. Dosanjh, R. Liang, and W. N. Hardy. Evidence for rapid suppression of quasiparticle scattering below t_c in $YBa_2Cu_3O_{7-\delta}$. *Physical Review Letters*, 68(15):2390–3, 1992.

[8] P. Bourges, H. Casalta, L. P. Regnault, J. Bossy, P. Burlet, C. Vettier, E. Beaugnon, P. Gautier-Picard, and R. Tournier. High magnetic field dependence of spin fluctuations in $YBa_2Cu_3O_7$. pages 830–1, 1997.

[9] S. D. Brorson, A. Kazeroonian, J. S. Moodera, D. W. Face, T. K. Cheng, E. P. Ippen, M. S. Dresselhaus, and G. Dresselhaus. Femtosecond room-temperature measurement of the electron-phonon coupling constant lambda in metallic superconductors. *Physical Review Letters*, 64(18):2172–5, 1990.

[10] S. L. Budko, G. Lapertot, C. Petrovic, C. E. Cunningham, N. Anderson, and P. C. Canfield. Boron isotope effect in superconducting MgB_2. *Physical Review Letters*, 86(9):1877–1879, 2001.

[11] J. P. Carbotte, E. Schachinger, and D. N. Basov. Coupling strength of charge carriers to spin fluctuations in high-temperature superconductors. *Nature*, 401(6751):354–6, 1999.

[12] M. Chiao, R. W. Hill, C. Lupien, B. Popic, R. Gagnon, and L. Taillefer. Quasiparticle transport in the vortex state of $YBa_2Cu_3O_{6.9}$. *Physical Review Letters*, 82(14):2943–6, 1999.

[13] J. M. Chwalek, C. Uher, J. F. Whitaker, G. A. Mourou, J. Agostinelli, and M. Lelental. Femtosecond optical absorption studies of nonequilibrium electronic processes in high t_c superconductors. *Applied Physics Letters*, 57(16):1696–8, 1990.

[14] J. M. Chwalek, C. Uher, J. F. Whitaker, G. A. Mourou, and J. A. Agostinelli. Subpicosecond time-resolved studies of coherent phonon oscillations in thin-film $YBa_2Cu_3O_{6+x}$ ($x<0.4$). *Applied Physics Letters*, 58(9):980–2, 1991.

[15] S. L. Cooper, A. L. Kotz, M. A. Karlow, M. V. Klein, W. C. Lee, J. Giapintzakis, and D. M. Ginsberg. Development of the optical conductivity with doping in single-domain $YBa_2Cu_3O_{6+x}$. *Physical Review B (Condensed Matter)*, 45(5):2549–52, 1992.

[16] S. L. Cooper, D. Reznik, A. Kotz, M. A. Karlow, R. Liu, M. V. Klein, W. C. Lee, J. Giapintzakis, D. M. Ginsberg, B. W. Veal, and A. P. Paulikas. Optical studies of the a-, b-, and c-axis charge dynamics in $YBa_2Cu_3O_{6+x}$. *Physical Review B (Condensed Matter)*, 47(13):8233–48, 1993.

[17] P. Dai, H. A. Mook, G. Aeppli, S. M. Hayden, and F. Dogang. Resonance as a measure of pairing correlations in the high-T_c superconductor $YBa_2Cu_3O_{6.6}$. *Nature*, 406(6799):965–8, 2000.

[18] P. Dai, H. A. Mook, S. M. Hayden, G. Aeppli, T. G. Perring, R. D. Hunt, and F. Dogan. The magnetic excitation spectrum and thermodynamics of high-T_c superconductors. *Science*, 284(5418):1344–7, 1999.

[19] J. Demsar. *Photoexcited Carrier Relaxation in High Temperature Superconductors probed by Ultrafast Optical Spectroscopy.* PhD thesis, University of Ljubljana, 2000.

[20] J. Demsar, R. Hudej, J. Karpinski, V. V. Kabanov, and D. Mihailovic. Quasiparticle dynamics and gap structure in $HgBa_2Ca_2Cu_3O_{8+\delta}$ investigated with femtosecond spectroscopy. *Physical Review B (Condensed Matter)*, 63:54519, 2001.

[21] J. Demsar, B. Podobnik, V. V. Kabanov, T. Wolf, and D. Mihailovic. Superconducting gap Δ_c, the pseudogap Δ_p, and pair fluctuations above t_c in overdoped $Y_{1-x}Ca_xBa_2Cu_3O_{7-\delta}$ from femtosecond time-domain spectroscopy. *Physical Review Letters*, 82(24):4918–21, 1999.

[22] J. N. Eckstein and I. Bozovic *Annual Reviews of Materials Science*, 25:679, 1995.

[23] G. L. Eesley, J. Heremans, M. S. Meyer, G. L. Doll, and S. H. Liou. Relaxation time of the order parameter in a high-temperature superconductor. *Physical Review Letters*, 65(27):3445–8, 1990.

[24] I. M. Fishman, G. S. Kino, X. D. Wu, W. R. Studenmund, and A. A. Abrikosov. Modulation measurements of $YBa_2Cu_3O_{7-x}$ optical reflectivity using a thermal wave technique. *Physica C*, 249(3-4):304–8, 1995.

[25] S. B. Fleischer, B. Pevzner, D. J. Dougherty, H. J. Zeiger, G. Dresselhaus, M. S. Dresselhans, E. P. Ippen, and A. F. Hebard. Ultrafast dynamics of superconducting K_3C_{60} and Rb_3C_{60}. *Physical Review B (Condensed Matter)*, 62(2):1366–78, 2000.

[26] H. F. Fong, P. Bourges, Y. Sidis, L. P. Regnault, A. Ivanov, G. D. Gul, N. Koshizuka, and B. Keimer. Neutron scattering from magnetic excitation in $Bi_2Sr_2CaCu_2O_{8+\delta}$. *Nature*, 398(6728):588–91, 1999.

[27] I. Y. Fugol, V. N.Samovarov, and M. Y. Libin. Dynamics of electronic excitations in YBCO at low temperatures. *Fizika Nizkikh Temperatur*, 25(5):459–468, 1999.

[28] P. Gay, D. C. Smith, C. J. Stevens, C. Chen, G. Yang, S. J. Abell, D. Z. Wang, J. H. Wang, Z. F. Ren, and J. F. Ryan. Femtosecond dynamics of BSCCO-2212. International Conference on Physics and Chemistry of Molecular and Oxide Superconductors. MOS'99 Stockholm, Sweden 28 July-2 Aug. 1999. pages 1025–9, 1999.

[29] S. G. Han, Z. V. Vardeny, O. G. Symko, G. Koren, G. L. Eesley, J. Heremans, M. S. Meyer, and G. L. Doll. Quasiparticle relaxation in a high- superconductor (comment and reply). *Physical Review Letters*, 67(8):1053–4, 1991.

[30] S. G. Han, Z. V. Vardeny, K. S. Wong, O. G. Symko, and G. Koren. Femtosecond optical detection of quasiparticle dynamics in high-T_c $YBa_2Cu_3O_{7-\delta}$ superconducting thin films. *Physical Review Letters*, 65(21):2708–11, 1990.

[31] W. N. Hardy, D. A. Bonn, D. C. Morgan, L. Ruixing, and Z. Kuan. Precision measurements of the temperature dependence of lambda in $YBa_2Cu_3O_{6.95}$: strong evidence for nodes in the gap function. *Physical Review Letters*, 70(25):3999–4002, 1993.

[32] M. J. Holcomb, J. P. Collman, and W. A. Little. Thermal difference spectroscopy. *Review of Scientific Instruments*, 64(7):1862–7, 1993.

[33] M. J. Holcomb, J. P. Collman, and W. A. Little. Optical evidence of an electronic contribution to the pairing interaction in superconducting $Tl_2Ba_2Ca_2Cu_3O_{10}$. *Physical Review Letters*, 73(17):2360–3, 1994.

[34] M. J. Holcomb, C. L. Perry, J. P. Collman, and W. A. Little. Thermal difference reflectance spectroscopy of high T_c superconductors. pages 606–16, 1996.

[35] B. Janko. Thermodynamic constraints on the magnetic field dependence of the neutron resonance in cuprate superconductors, Los Alamos Preprint Arhives. 2000.

[36] V. V. Kabanov, J. Demsar, B. Podobnik, and D. Mihailovic. Quasiparticle relaxation dynamics in superconductors with different gap structures: Theory and experiments on $YBa_2Cu_3O_{7-\delta}$. *Physical Review B (Condensed Matter)*, 59(2):1497–506, 1999.

[37] R. A. Kaindl. *Ultrafast mid-infrared studies of low-energy excitations in solids*. PhD thesis, Humboldt-Universtat zu Berlin, 2000.

[38] R. A. Kaindl, F. Eickemeyer, M. Woerner, and T. Elsaesser. Broadband phase-matched difference frequency mixing of femtosecond pulses in GaSe: Experiment and theory. *Applied Physics Letters*, 75(8):1060–2, 1999.

[39] R. A. Kaindl, D. C. Smith, M. Woerner, C. J. Stevens, G. A. Wagner, J. E. Evetts, J. F. Ryan, and T. Elsaesser. Ultrafast mid-infrared response of nonequilibrium excitations in the high T_c superconductor $YBa_2Cu_3O_{7-\delta}$. pages 120–1, 1999.

[40] R. A. Kaindl, M. Woerner, T. Elsaesser, D. C. Smith, J. F. Ryan, G. A. Farnan, M. P. McCurry, and D. G. Walmsley. Ultrafast mid-infrared response of $YBa_2Cu_3O_{7-\delta}$. *Science*, 287(5452):470–3, 2000.

[41] R. Liang, D. A. Bonn, and W. N. Hardy. Preparation and x-ray characterization of highly ordered ortho-II phase $YBa_2Cu_3O_{6.50}$ single crystals. *Physica C*, 336(1-2):57–62, 2000.

[42] R. Liang, P. Dosanjh, D. A. Bonn, D. J. Baar, J. F. Carolan, and W. N. Hardy. Growth and properties of superconducting ybco single crystals. *Physica C*, 195(1-2):51–8, 1992.

[43] M. Lindgren, M. Currie, C. Williams, T. Y. Hsiang, P. M. Fauchet, R. Sobolewski, S. H. Moffat, R. A. Hughes, J. S. Preston and F. A. Hegmann. Intrinsic picosecond response times of Y-Ba-Cu-O superconducting photodetectors. *Applied Physics Letters*, 74(6):853–5, 1999.

[44] Y. E. Lozovik, A. L. Dobryakov, N. P. Ernsting, and S. A. Kovalenko. New method of non-fermi liquid study by pump-supercontinuum probe femtosecond spectroscopy. *Physics Letters A*, 223(4):303–7, 1996.

[45] R. P. Mallozzi. *High-frequency electrodynamics of cuprate superconductors*. PhD thesis, University of California-Berkeley, 1998.

[46] C. May, R. W. Hill, C. Lupien, L. Taillefer, P. Lambert, R. Gagnon, and P. Fournier. Low-energy quasiparticles in cuprate superconductors: A quantitative analysis. *Physical Review B (Condensed Matter)*, 62(5):3554–8, 2000.

[47] I. I. Mazin, A. I. Liechtenstein, O. Jepson, O. K. Andersen, and C. O. Rodriguez. Displacive exitation of coherent phonons in YBa_2Cu_3O. *Physical Review B (Condensed Matter)*, 49(13):9210–13, 1994.

[48] D. Mihailovic and J. Demsar. Time-resolved optical studies of quasiparticle dynamics in high-temperature superconductors. In E. Faulques, editor, *Spectroscopy of Superconducting Materials*, volume 730 of *ACS Symposium Series*. 1999.

[49] O. V. Misochko, K. Sakai, and S. Nakashima. Femtosecond pump-probe study of $YBa_2Cu_4O_8$ superconductor. *Physica C*, 329(1):12–16, 2000.

[50] K. A. Moler, D. J. Baar, J. S. Urbach, L. Ruixing, W. N. Hardy, and A. Kapitulnik. Magnetic field dependence of the density of states of $YBa_2Cu_3O_{6.95}$ as determined from the specific heat. *Physical Review Letters*, 73(20):2744–7, 1994.

[51] D. Munzar, C. Bernhard, and M. Cardona. Does the peak in the magnetic susceptibility determine the in-plane infrared conductivity of ybco? a theoretical study. *Physica C*, 312(1-2):121–35, 1999.

[52] D. Munzar, C. Bernhard, and M. Cardona. Possible relationship between the peak in the magnetic susceptibility and the in-plane far-infrared conductivity of YBCO. First Euroconference on Anomalous Complex Superconductors Crete, Greece 26 Sept.-3 Oct. 1998 pages 547–9, 1999.

[53] C. I. Perry, M. J. Holcomb, J. P. Collman, and W. A. Little. Experimental studies of the high-temperature superconducting cuprates using thermal difference reflectance spectroscopy. pages 664–71, 1996.

[54] W. H. Press. *Numerical recipes in C : the art of scientific computing.* Cambridge University Press, Cambridge Cambridgeshire ; New York, 2nd , rev. edition, 1997.

[55] C. Renner, B. Revaz, K. Kadowaki, I. Maggio-Aprile, and O. Fischer. Observation of the low temperature pseudogap in the vortex cores of $Bi_2Sr_2CaCu_2O_{8+\delta}$. *Physical Review Letters*, 80(16):3606–9, 1998.

[56] A. Rothwarf and B. N. Taylor. measurement recombination lifetimes in superconductors. *Physical Review Letters*, 19(1):27–30, 1967.

[57] L. D. Rotter, Z. Schlesinger, R. T. Collins, F. Holtzberg, C. Field, U. W. Welp, G. W. Crabtree, J. Z. Liu, Y. Fang, K. G. Vandervoort, and S. Fleshler. Dependence of the infrared properties of single-domain $YBa_2Cu_3O_{7-y}$ on oxygen content. *Physical Review Letters*, 67(19):2741–4, 1991.

[58] Z. Schlesinger, R. T. Collins, F. Holtzberg, C. Feild, S. H. Blanton, U. Welp, G. W. Crabtree, Y. Fang, and J. Z. Liu. Superconducting energy gap and normal-state conductivity of a single-domain $YBa_2Cu_3O_7$ crystal. *Physical Review Letters*, 65(6):801–4, 1990.

[59] R. W. Schoenlein, W. Z. Lin, J. G. Fujimoto, and G. L. Eesley. Femtosecond studies of nonequilibrium electronic processes in metals. *Physical Review Letters*, 58(16):1680–3, 1987.

[60] J. L. W. Siders, R. N. Jacobs, C. W. Siders, S. A. Trugman, and S. A. Taylor. Nonequilibrium superconductivity and quasiparticle dynamics in $YBaCu_30_{7-\delta}$. In T. Elsaesser, editor, *Ultrafast Phenomena XI*, pages 365–367. Springer Verlag, 1998.

[61] D. C. Smith, P. Gay, C. J. Stevens, D. Z. Wang, J. H. Wang, Z. F. Ren, and J. F. Ryan. Ultrafast optical response of $Tl_2Ba_3CuO_{6+\delta}$. International Conference on Physics and Chemistry of Molecular and Oxide Superconductors. MOS'99 Stockholm, Sweden 28 July-2 Aug. 1999. pages 1059–63, 1999.

[62] C. J. Stevens, P. Gay, D. C. Smith, C. Chen, and J. F. Ryan. Anisotropy of the non-equilibrium quasiparticle dynamics in single crystals of $YBa_2Cu_3O_{7-\delta}$. International Conference on Physics and Chemistry of Molecular and Oxide Superconductors. MOS'99 Stockholm, Sweden 28 July-2 Aug. 1999. pages 1031–5, 1999.

[63] C. J. Stevens, D. Smith, C. Chen, J. F. Ryan, B. Podobnik, D. Mihailovic, G. A. Wagner, and J. E. Evetts. Evidence for two-component high-temperature superconductivity in the femtosecond optical response of $YBa_2Cu_3O_{7-\gamma}$. *Physical Review Letters*, 78(11):2212–15, 1997.

[64] W. R. Studenmund, I. M. Fishman, G. S. Kino, and J. Giapintzakis. Symmetry of differential optical responses of normal and superconducting phases in single-crystal YBCO. Conference on Spectroscopies in Novel Superconductors Stanford, CA, USA 15-18 March 1995. pages 1843–4, 1995.

[65] W. R. Studenmund, I. M. Fishman, G. S. Kino, and J. Giapintzakis. Progress in photothermal microscopy of $YBa_2Cu_3O_{7-x}$. Spectroscopies in Novel Superconductors Cape Cod, MA, USA 14-18 Sept. 1997. pages 2012–14, 1998.

[66] A. J. Taylor, G. Rodriguez, J. L. W. Siders, C. W. Siders, and S. A. Trugman. Nonequilibrium superconductivity and quasiparticle dynamics in $YBa_2Cu_3O_{7-\delta}$. Quantum Electronics and Laser Science Conference Baltimore, MD, USA 23-28 May 1999. pages 118–19, 1999.

[67] T. N. Thomas, C. J. Stevens, A. J. S. Choudhary, J. F. Ryan, B. Mihailovic, T. Mertelj, L. Forro, G. Wagner, and J. E. Evetts. Photoexcited carrier relaxation and localization in $Bi_2Sr_2Ba_{1-y}$ $Y_yCu_2o_8$ and $YBa_2Cu_3O_{7-\delta}$: a study by femtosecond time-resolved spectroscopy. *Physical Review B (Condensed Matter)*, 53(18):12436–40, 1996.

[68] M. Tinkham. *Introduction to superconductivity*. International series in pure and applied physics. McGraw Hill, New York, 2nd edition, 1996.

[69] C. C. Tsuei, J. R. Kirtley, Z. F. Ren, J. H. Wang, H. Raffy, and Z. Z. Li. Pure $d_{x^2-y^2}$ order-parameter symmetry in the tetragonal superconductor $Tl_2Ba_2CuO_{6+\delta}$. *Nature*, 387(6632):481–3, 1997.

[70] J. R. Waldram. *Superconductivity of metals and cuprates*. Institute of Physics Pub., Bristol ; Philadelphia Pa., 1996.

[71] M. B. Walker and M. F. Smith. Quasiparticle-quasiparticle scattering in high-T_c superconductors. *Physical Review B (Condensed Matter)*, 61(17):11285–8, 2000.

[72] D. A. Wollman, D. J. Van Harlingen, W. C. Lee, D. M. Ginsberg, and A. J. Leggett. Experimental determination of the superconducting pairing state in YBCO from the phase coherence of YBCO-Pb dc squids. *Physical Review Letters*, 71(13):2134–7, 1993.

Appendix A

Aligning Tips

This section is intended as reference for those who choose to undertake similar experiments but lack the expertise to setup an optical system. There are a number of important steps in the alignment process and some of the "tricks" are described below.

A useful overall design consideration is to set the probe beam and consider it fixed and make adjustments to the pump beam as necessary. Additionally any modulations are made only to the pump arm, it has the rapid scan delay and the photoelastic modulator. In this way the probe signal has a very stable DC background.

A.1 Delay Lines

The optical delay line may be oriented by using a razor blade to block half of the reflected beam. Any modulation of the beam intensity measured by a power meter and observed on an oscilloscope is an indication that the travel of the delay line is not parallel to the beam. Deviations for the vertical and horizontal orientations of the blade should be

simultaneously minimized. The figure of merit is the fluctuation of the beam intensity that occurs when the power is reduced by half of its maximum. We achieved variations of less than .5% for a range of travel which greatly exceeded the range of travel of interest.

The alignment of the stepper (Klinger) in the probe arm is much less critical, as it is not moving during data acquisition. A proper alignment requires two steps, however. Care must be taken to ensure the retroreflector which is manually adjusted performs its job of reflecting the beam along a parallel path. This is accomplished by covering half of the second reflecting surface and translating the mirror. The goal is the same as before, minimize changes in the reflected power.

A.2 Finding the Overlap

Once the pump and probe beams are co-propagating, it is a good idea to ensure that they are parallel and at the same height. The probe beam is then focussed through the optic axis of the lens. Using a pinhole or razor blade mounted on a translation stage and a power meter, the position of the beam waist should be determined. The probe beam is then blocked and the pump beam is then adjusted so as to maximize the pinhole throughput. Some experiments have used larger pump and smaller probe beams. This configuration can probe a region of more uniform excitation density.

Another useful method for checking overlap and the extent to which the pump beam is scattering into the probe beam is to place a card with two small holes in it to allow the incident beams to pass into the cryostat. The return beams should then hit the card (on the opposite side) upon reflection from the sample, provided the beams are nearly

normally incident on the sample surface. Using the translation stage to move the sample in a direction perpendicular to the beam path while simultaneously observing the reflected light will reveal small variations in the surface morphology. A precise synchronization of these variations in the two beams indicates good overlap. Delayed or uncorrelated variations mean adjustment is required.

Once a pump probe signal is obtained, we steer the pump beam, using a mirror mount with fine pitch screws so that the signal is maximized.

Appendix B

Supplementary Data

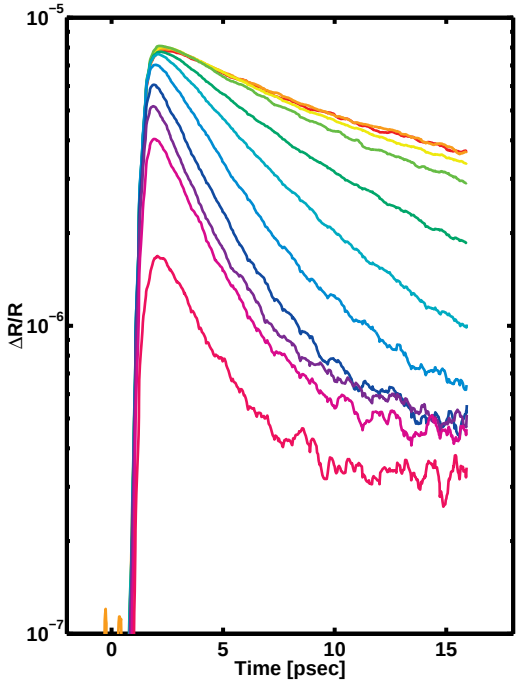

Figure B.1: Optimal doped BSCCO plotted on a semilog axis, showing the dominant single exponential character of the decay kinetics.

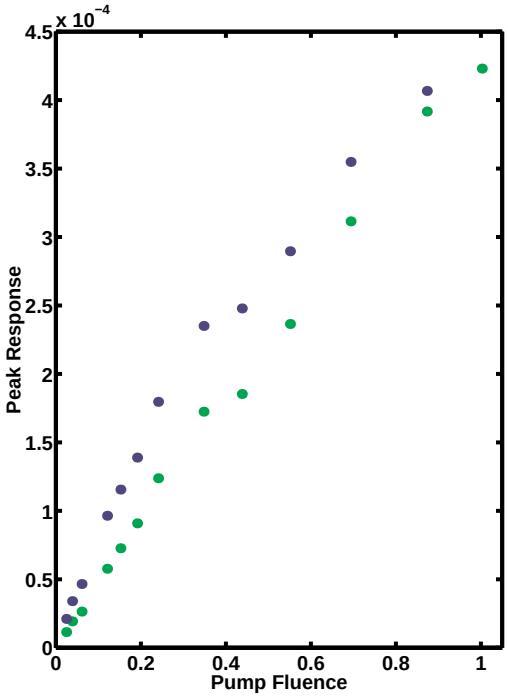

Figure B.2: YBCO: Peak response *vs* pump fluence. Peak pump power is 25mW focused to a 80μ diameter spot. Underdoped is blue, optimal is green. Note sublinear behavior for the highest fluences. T=10K.

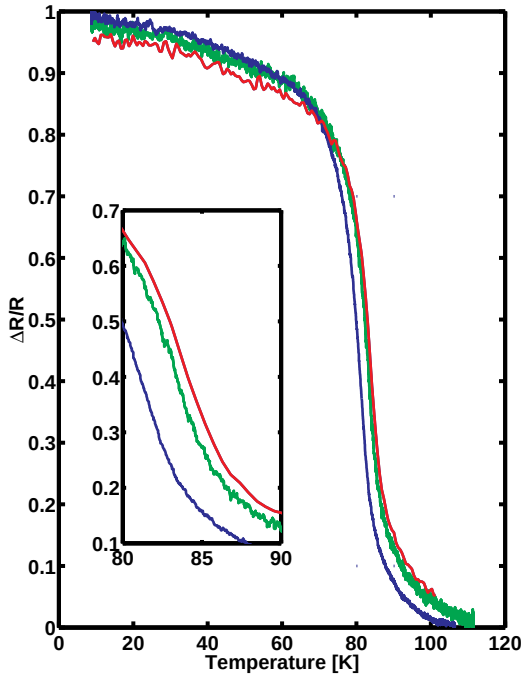

Figure B.3: Comparison of three pump fluences on a temperature swept curve (optimally doped from YBCO). Pump fluence is approximately .1(red), .03(green), .012(blue). The inset magnifies the transition region, revealing the shift most clearly. T_c=89K as measured by SQUID. The temperature of the probe spot may differ substantially from the temperature sensor at high pump fluences.

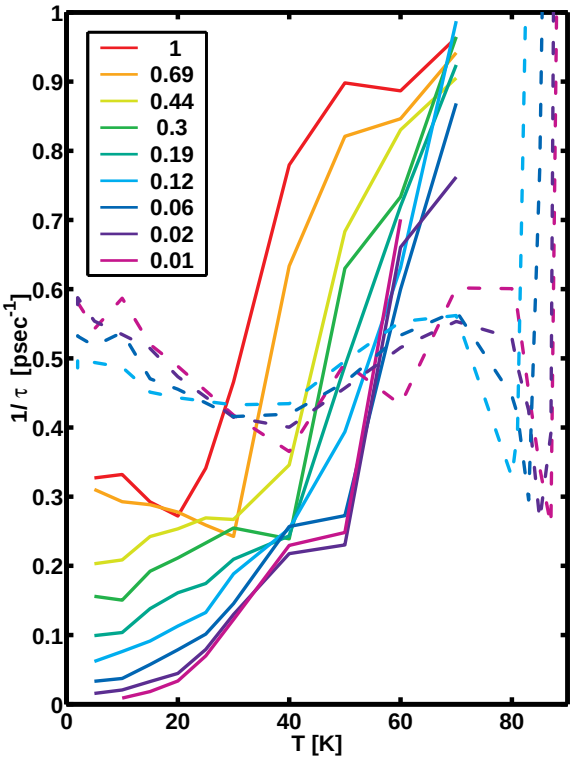

Figure B.4: Extracted decay rate for underdoped(solid) and optimal(dashed) YBCO plotted *vs* temperature for different pump fluences. In optimal, the recombination rate is insensitive to temperature whereas large variations in the lifetime are apparent in the underdoped sample. The time interval fit was between 95% and 70% of the maximum.